Appendix 5.

APPROXIMATE METHOD TO DETERMINE THE PEELING STRESS IN MATTRESS-LIKE PROTECTION AIRBAGS

Contents

19. INTRODUCTION

The strength analysis of a protective airbag is a complicated and painstaking task.

From the mechanical standpoint, the airbag is a nonlinearly deformable shell made of a soft material; the shell contains hollows filled by gas, experiences large displacements, and allows unstable folds to appear in it and interact with one another. Systems of this kind are analyzed by iterative methods using finite element techniques.

The calculations for this type of analysis require a lot of preparations and substantial computing resources. The process of solution needs to be permanently monitored by an analyst.

To obtain a quick estimation of an airbag design in the course of a multi-variant development procedure, it would be helpful to have an approximate method of analysis giving a fast and relatively informative result.

This report describes an attempt of creation and further improvement of such an approximate method.

The method has been tested by some real examples and validated by its comparing with results obtained by the finite element analysis.

1. PRINCIPLES OF APPROXIMATE METHOD

1.1. Integral representation of the peeling forces

Let us consider an example from the paper [23] illustrated by Fig. 1.1. Let's select a segment *AB* on the contour of the adhesive joint and set the goal to determine the peeling stress that acts on this segment.

With this purpose, we draw a line *ACDB* on the surface of the shell, that connects the ends of the segment. The principle of its construction will be explained below. Let *AEFB* be a projection of this line onto the horizontal symmetry plane of the shell. We cut a spatial fragment *ABCDEF* from the shell filled with gas, bounded by the shell's surface fragment *ACDB* from above, by the projection *AEFB* from below, and by a surface extended over vertical lines which connect points of the *ACDB* line and those of its projection on its sides. The action of the rest of the shell will be replaced by forces applied to the cut fragment. To determine the desirable peeling stress, we sum projections of all forces applied to the fragment onto the vertical axis and equate it to zero.

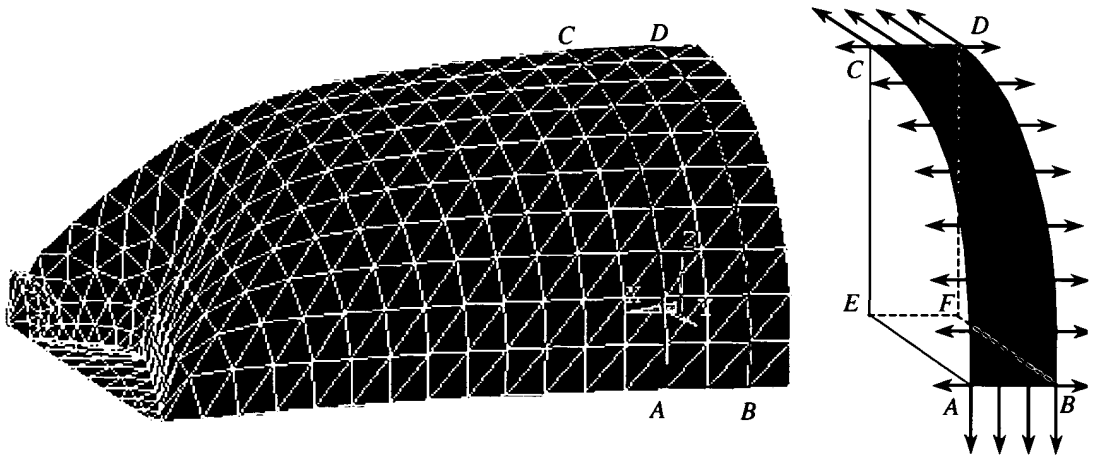

Fig. 1.1. To an integral representation of the peeling force

The key point in the construction above follows. The *ACDB* line should be built in such way that the resultant of forces replacing the removed part of the shell be horizontal on any infinitesimal segment of the *ACDB* line. As the forces that replace the gas pressure on the side surface of the extracted spatial fragment are also horizontal, the equilibrium equation will contain two terms only:

(1.1) $pS - N_{AB} = 0;$

where p is the gas pressure above ambient inside the shell;

S is the area of the projection of the *ACDB* surface fragment onto the horizontal plane;

N_{AB} is the peeling force that arises on the *AB* segment.

It follows from the formula (1.1) that:

(1.2) $N_{AB} = pS.$

Generally, in this way we can find the outline of the area from which the load is transferred to any segment of the adhesive joint contour. Passing to an infinitesimal length dl of this segment, we have an outline of an infinitesimal area dS which enables us to determine the peeling stress by a simple formula:

(1.3) $$\psi = p\frac{dS}{dl}.$$

We can derive differential equations to determine the accurate position of this area's boundary. But we will do it in a different way. We take only the idea and the formulae of the method described above.

The boundaries of the load transfer areas will be determined on the basis of plausible assumptions. Using these boundaries, we will calculate the area of the load transfer, and then use the formulae (1.2) and (1.3) to find the desirable values. The results thus obtained will be compared to results obtained with analytical or numerical methods. The feasibility criterion of the approximate method will be a proximity of the results.

1.2. General principle

Let's divide the contour of the adhesive joint between the sheets the airbag is made of, into a finite or infinite number of segments arbitrarily chosen using considerations of any kind. The ideas of Section 1.1 lead us to a conclusion that the horizontal projection of the inflated bag can be divided into areas so that each segment correspond to an area from which the load is transferred to a given segment of the joint's contour.

The principle of dividing the whole region into areas follows: **we assume any point of the region to transfer the load to a contour's segment nearest to it and to belong to the area that corresponds to the segment**.

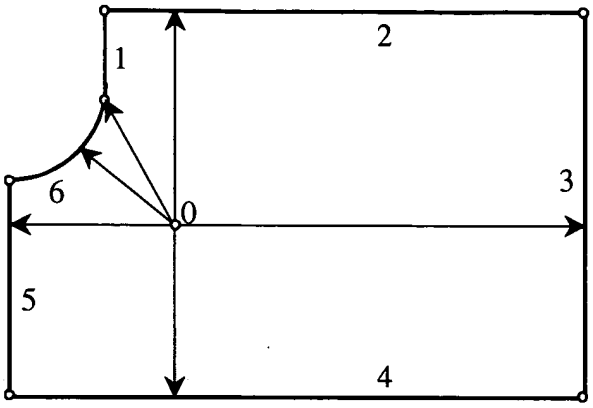

Fig. 1.2. The distance from point 0 to segments of the contour

The remoteness of a particular point is measured by the distance from it to the nearest point of the contour's segment. Fig. 1.2 presents an example. The joint's contour is divided into six segments denoted in Fig. 1.2 by integer numbers from 1 to 6. Arrows show the distances from the point 0 to the segments of the contour. The drawing makes it clear the point 0 belongs to an area that corresponds to the segment 6.

If a point is equidistant from two contour segments, then it belongs to a boundary of areas that correspond to these two segments. A segment of the boundary between two areas can be defined as a locus of points equidistant from two respective segments of the joint's contour.

1.3. Boundaries of areas

In most cases the joint's contour consists of segments representing straight lines and circular arcs. Let's discuss the construction of curves equidistant from couples of the said lines.

If both segments are rectilinear, their equidistant line is a bisectrix of an angle between the two segments that crosses their intersection point. The point may belong to both segments, one or none of them. If the segments are parallel, the equidistant line is parallel to them and is exactly between the lines of the segments.

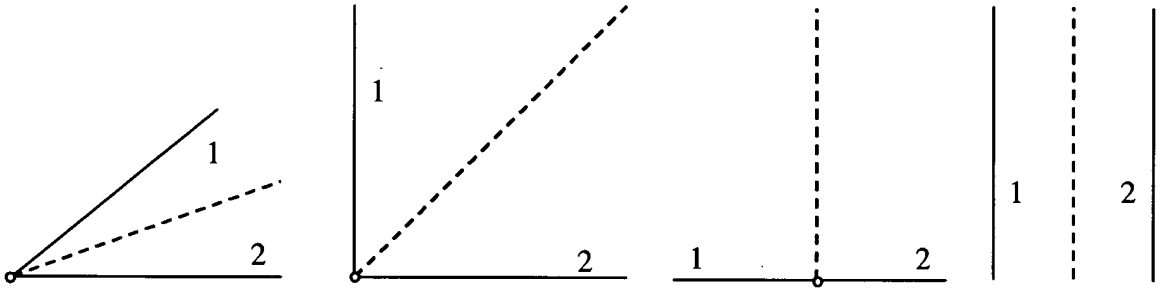

Fig. 1.3. Equidistant lines of two straight lines

If one of the lines is straight while the second one is a circle, their equidistant line will be a parabola with its axis perpendicular to the straight line and its focus at the center of the circle (Fig. 1.4).

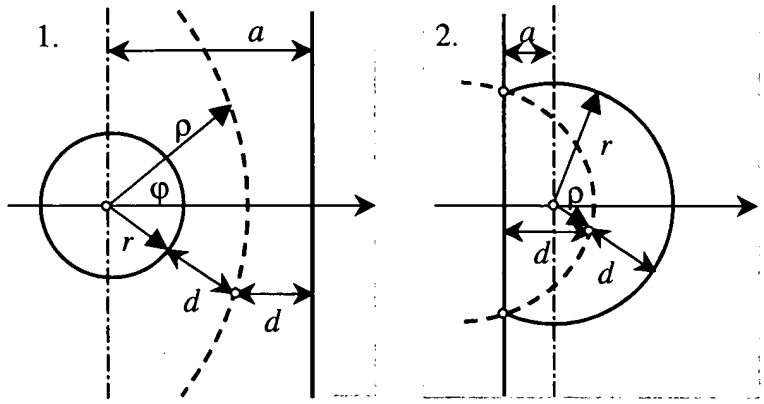

Fig. 1.4. A line equidistant from a straight line and a circle

Where there is a circular contour, it is convenient to use a polar coordinate system with its origin at the center of the circle. The equation of an equidistant parabola shown as a dash line in Fig. 1.4.1 in polar coordinates follows:

$$(1.4) \qquad \rho = \frac{a+r}{1+\cos\varphi}.$$

The distance from a point of the parabola to the circle (equal to the distance from the same point to the straight line) is expressed by the formula:

$$(1.5) \qquad d = \frac{a-r\cos\varphi}{1+\cos\varphi}.$$

Signs of the coefficients in the formulae (1.4) and (1.5) can change depending on a mutual arrangement of the circle and the line. Also, they depend on whether we consider the exterior or interior area with respect to the circle (see Fig. 1.4.1 and Fig. 1.4.2).

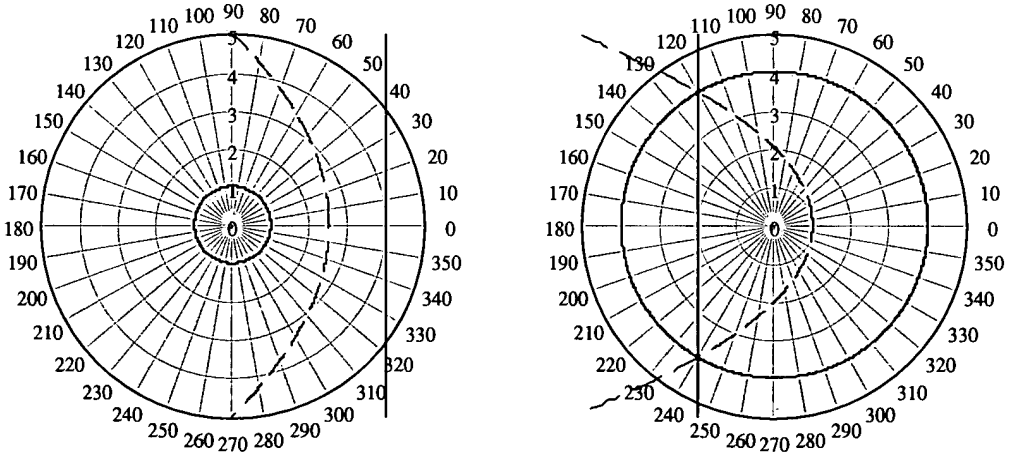

Fig. 1.5. A mathematical construction of equidistant lines of a line and a circle, in exterior and interior areas

If both curves are circles, then their equidistant line can be a hyperbola, a straight line, or an ellipse. In an exterior area with respect to both circles is under consideration, then generally this equidistant line will be a hyperbola (Fig. 1.6). When both circles have equal radii, the hyperbola degenerates into a straight line. Of two branches of the hyperbola, one the focus of which is at the center of the circle with a less radius is to be chosen.

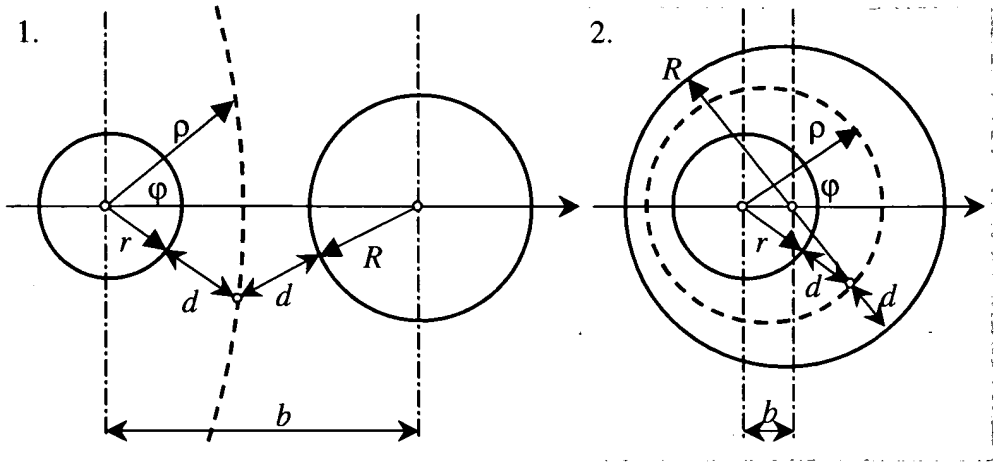

Fig. 1.6. A line equidistant from two circles

The equation of this hyperbola is:

$$(1.6) \qquad \rho = \frac{b}{2e} \cdot \frac{(e^2 - 1)}{1 + e\cos\varphi};$$

where $e = \frac{b}{R - r} > 1$ is the eccentricity of the hyperbola;

b is the distance between the centers of the circles;

$R > r$ are the radii of the circles.

The distance from the hyperbola (Fig. 1.6.1) to the circles is a function of the angle φ and can be expressed by the formula:

$$(1.7) \qquad d = \frac{b}{2e} \cdot \frac{(e^2 - 1)}{1 + e\cos\varphi} - r.$$

If an area exterior for one circle and interior for the other one is under consideration, then an ellipse will be their equidistant line. The equation of the ellipse is:

$$(1.8) \qquad \rho = \frac{b}{2e} \cdot \frac{1 - e^2}{1 - e\cos\varphi};$$

where $e = \frac{b}{R + r}$ is the ellipse's eccentricity;

b is the distance between the centers of the circles;

$R > r$ are the radii of the circles.

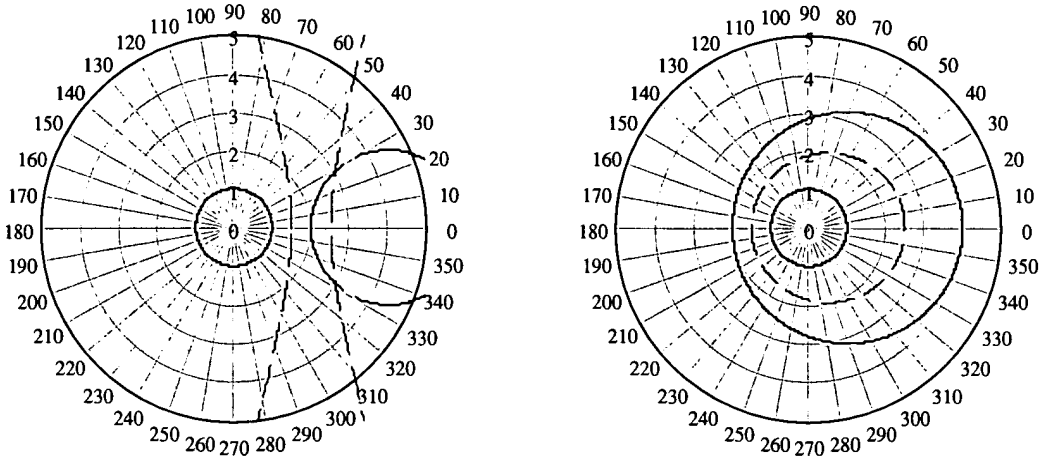

Fig. 1.7. A mathematical construction of equidistant lines of two circles for exterior and interior areas with respect to the circle of a greater radius

The distance from the ellipse (Fig. 1.6.2) to the circles is a function of the angle φ expressed by the formula:

$$(1.9) \qquad d = \frac{b}{2e} \cdot \frac{1-e^2}{1-e\cos\varphi} - r.$$

1.4. Division of a contour into segments and a region into areas

To solve a particular problem, at the first stage it is convenient to divide the contour of a region into segments, each one being a primitive: a piece of a straight line, a circular arc, an arc of another curve, a point etc. Fig. 1.8 presents an example of a division of this kind. Numbers of the contour's segments are designated by boldface outside the contour. Segments 1,..,5 are straight lines, segment 6 is a circular arc.

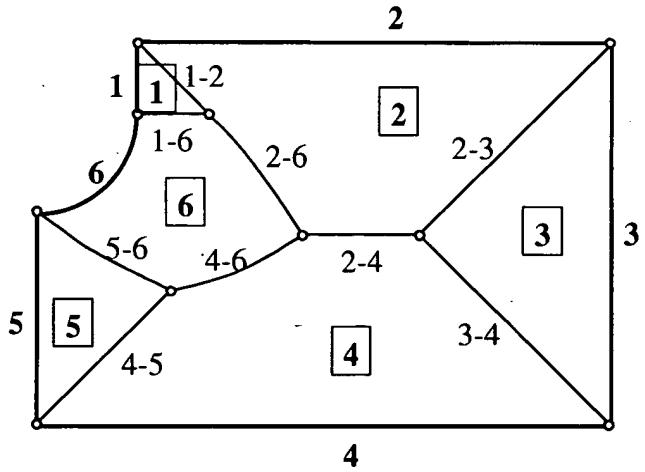

Fig. 1.8. An example of a region divided into areas according to its contour's division into primitives

Using the main principle and the relationships given in Section 1.3, we can divide the whole region into areas according to the way the contour is divided into primitives. This division for the example being considered is shown in Fig. 1.8. Number of the region's areas are designated by digits in rectangular frames. Interior boundaries of the areas consist of straight lines and parabolic arcs. The

latter are denoted by couples of digits. The boundaries 2-6, 4-6, 5-6 are parabolic arcs. The rest are segments of straight lines.

In some points three (or more) boundaries of areas meet. These interior points of the region are denoted by small circles on the drawing. The points are equidistant from three (or more) segments of the contour.

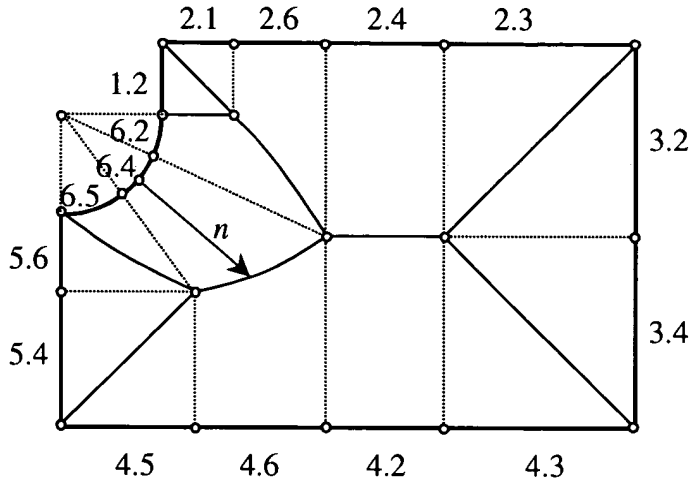

Fig. 1.9. An example of a division of areas into sub-areas and the contour's segments into sub-segments

The next stage is to divide the areas into sub-areas and, respectively, the contour's segments into sub-segments. The goal of this operation is to ensure that the peeling stress at each sub-segment is determined by a single formula. The normal raised from any point of a sub-segment of the contour must reach the same segment of the boundary between the areas. This stage will become clearer after considering an example of the division shown in Fig. 1.9.

It is convenient to denote the sub-segments by codes consisting of two numbers. The first part of the code is No. of the segment, and its second part is No. of the area the boundary of which is hit by the normal. Fig. 1.9 shows a normal raised up from a point of the sub-segment 6.4. This normal hits the boundary of the area 4.

20. DETERMINING THE PEELING STRESS

20.1. Main formula derivation

The formula (1.3) can be used to determine the peeling stress. This formula includes the pressure above ambient in the shell p, the length of an infinitesimal contour segment dl, and the area of the area dS that corresponds to this segment.

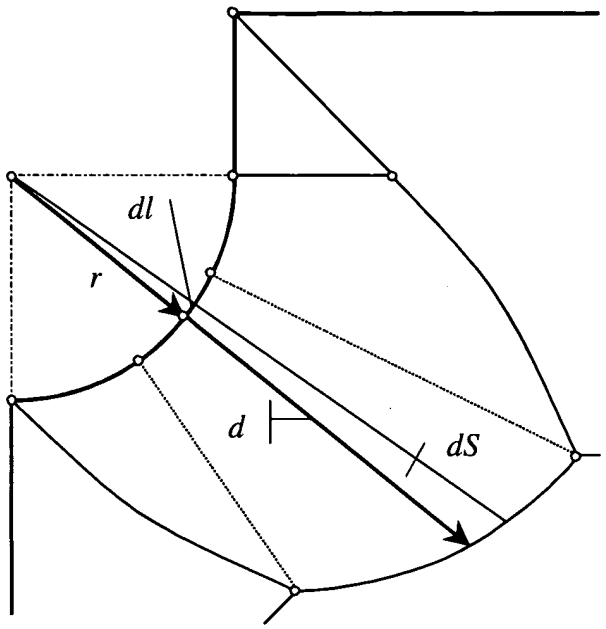

Fig. 20.1. To the determination of the peeling stress

Fig. 20.1 shows a segment of a curvilinear contour with its curvature radius r, the convexity of which is directed inwards the area. On this contour an infinitesimal segment of the length dl is selected. This segment corresponds to an area dS painted in Fig. 20.1. It's easy to see that the area is equal to

$$dS = d(1+\frac{d}{2r})dl. \qquad (20.1)$$

Here d is the length of a normal from the contour line to the area's boundary.

Now we have all data needed to calculate the peeling stress by the formula (1.3).

Using the contour's curvature instead of its curvature radius,

$$\kappa = \frac{1}{r}; \qquad (20.2)$$

we can rewrite the formula (1.3) for the peeling stress ψ as:

$$\psi = pd\left(1+\frac{\kappa d}{2}\right). \qquad (20.3)$$

One should note that the curvature is positive when the curve's convexity looks inwards the area. If it looks outwards, the curvature is negative.

At rectilinear segments of the contour where $\kappa = 0$, the formula (20.3) becomes simpler:

$$\psi = pd. \qquad (20.4)$$

Thus, the normal length d plays a key role in the determination of the peeling stress on the contour.

A special case is represented by a salient point on the contour looking inwards the area with its sharp end. The curvature of the contour in the vicinity of this point tends to infinity, so does the peeling stress. Though, the peeling stress resisted by the vicinity of the salient point is finite. It can be determined by the value of an area that surrounds the salient point. The outline of the area is defined by the common rules if the salient point is treated as a separate segment of the contour.

20.2. An analogy of an equally sloped roof

Let's imagine how somebody has built a house the plan of which matches the shape of the area of interest (on a larger scale). Exterior walls of the house have the same height and follow exactly the contour of the area. They have decided to make the roof of the house have a pitch t, as it is a usual way to do. What will the shape of this roof be?

The pitch of the roof that adjoins a rectilinear segment of the contour will be an inclined plane with the slope t. The pitch that joins a circular arc segment the convexity of which looks inwards will be a cone with its axis vertical, the slope of its generatrix equal to t, and its vertex looking downwards. The pitch that joins a circular arc segment the convexity of which looks outwards will be a cone with its axis vertical, the slope of its generatrix equal to t, and an upward-looking vertex.

When these surfaces are extended inwards the building up to lines where they cross, we will have the whole surface of the roof. The lines of their intersection are boundaries of the above-stated areas. That's why Fig. 1.8 resembles a plan of an equally pitched roof. When it rains, streams of water flow over the roof from its center to its periphery eventually crossing the contour of the building. Each segment of the contour is crossed by certain amount of water.

Suppose it has rained with an intensity p, i.e. p kg of water has fallen on each square meter of the horizontal surface. All water has flown down from the roof crossing its contour. In this case the weight of water that has crossed a unit of the contour's length will be equal to the peeling stress in the respective location of the airbag.

20.3. A practical method of determining the peeling stress

The considerations above relate to the shape of the airbag filled with air. But this shape is not known beforehand.

The suggested method is approximate anyway, therefore let's make another assumption. We are going to perform all geometrical constructions with the flat base of the airbag, and then make a transition to the deformed state by introducing correction coefficients into formulae of the peeling stress.

Two correction coefficients are suggested:

k_g , being a global coefficient to allow for the difference between the area of the horizontal projection of the filled airbag's hollow and the area of the same hollow in the flat base;

k_l , being a local coefficient to allow for deviations of the real stress from its approximate value in a local area of the airbag.

The global coefficient is the same for the whole airbag. It is to be determined from the condition that the sum of the peeling forces in the approximate calculation be equal to the sum of the peeling forces in the reality. The local coefficients may vary over the hollow's contour.

The following technique of an approximate peeling stress calculation is feasible. First, put a scheme of the hollow's division into areas with a pencil right on the flat airbag. An example of this is Fig. 1.8. Then, mark points of the contour on the same drawing where the stress is to be found. Next, measure the length of the normal d in each point with a rule (см. Fig. 20.1), and use the drawing to find the contour's curvature radius r in this point.

Having done all this, find the peeling stress by the formula

$$\psi = k_g k_l p d \left(1 + \frac{d}{2r}\right) \qquad (20.5)$$

for curvilinear segments of the contour, and by the formula

$$\psi = k_g k_l p d \qquad (20.6)$$

for rectilinear segments.

The coefficients k_g and k_l must be tabulated by solving a good deal of problems.

Right now, we can say the coefficient k_g varies in the range 0.6 to 0.7 and can be tentatively assumed 0.65.

The coefficient k_l needs a careful study.

21. COMPARISON OF RESULTS

This chapter presents a comparison of results of calculations performed by the approximate technique with those obtained analytically or by the finite element analysis and reported in [23].

21.1. A cylindrical hollow

The appendix [23] deals with the behavior of an infinitely long cylindrical hollow filled with gas (see Fig. 21.1). The base of this hollow consists of two strips of a soft material $2a$ wide tied together by flank adhesive joints. There is gas at the pressure p above ambient inside the hollow. If the material is non-deformable and the hollow is not subject to a lateral tension ($q_1 = 0$), then the peeling stress in the flank seams is expressed by the formula:

(21.1) $$\psi = \frac{2}{\pi} pa .$$

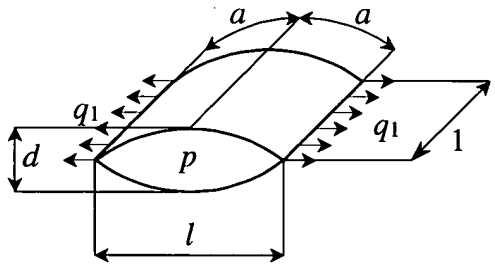

Fig. 21.1. A schematic of a cylindrical hollow

The area of the base is divided into two obvious areas as shown in Fig. 21.2. The length of the normal to the contour is a.

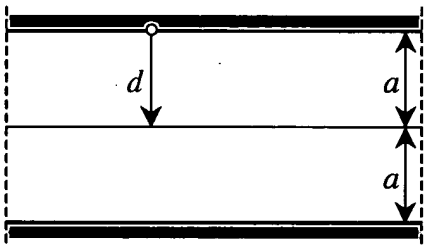

Fig. 21.2. The base region divided into areas

According to the technique suggested here, the peeling stress can be calculated approximately by the formula (20.6):

(21.2) $$\psi = k_g k_l pa .$$

The formulae (21.1) and (21.2) have the same structure, and the formula (21.2) yields an accurate result if we adopt the following correction coefficients:

(21.3) $$k_g = \frac{2}{\pi} = 0.64; \qquad k_l = 1.0.$$

Thus, the peeling stress in the flank seams of a cylindrical hollow can be determined accurately by to the suggested technique, adopting the correction coefficients as in (21.3).

21.2. An annular hollow

The appendix [23] deals with the behavior of an annular hollow (see Fig. 21.3). The base of this hollow consists of two circles of a soft material of the radius b that have an annular adhesive joint along their contours and a central joint of a circular shape with the radius a. There is gas under the pressure p above ambient inside the hollow.

Let's divide the contour's boundary into two segments: an interior contour and an exterior contour. The curvature of the interior contour is positive and equal to $1/a$. That of the exterior contour is negative and equal to $1/b$. The respective division of the hollow into areas is shown in Fig. 21.3. The areas have the shapes of rings with the width

(21.4) $$d = \frac{b-a}{2}.$$

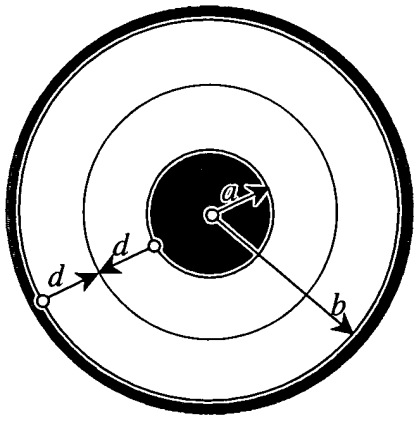

Fig. 21.3. A division of the annular hollow into areas

According to the proposed technique, the peeling stress can be calculated approximately by the formulae (20.5). For the interior contour this formula is

(21.5) $$\psi^i = k_g k_l^i pd\left(1+\frac{d}{2a}\right).$$

For the exterior contour it is slightly different:

(21.6) $$\psi^o = k_g k_l^o pd\left(1-\frac{d}{2b}\right).$$

On the basis of results presented in [23], we can build plots of the coefficients k_g, k_l^i, k_l^o which will yield approximate solutions almost identical with the accurate ones. These coefficients depend on a dimensionless parameter

(21.7) $$\eta = \frac{d}{a};$$

that characterizes the relative curvature of the interior contour.

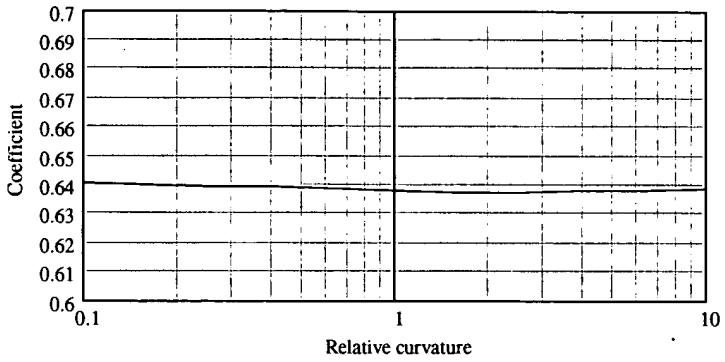

Fig. 21.4. A dependence of the coefficient k_g vs. relative curvature η

Fig. 21.4 presents a plot of the coefficient k_g vs. the relative curvature η. As one can see on this plot, the coefficient is pretty stable and can be assumed $k_g = 0.64$ independently from the relative curvature.

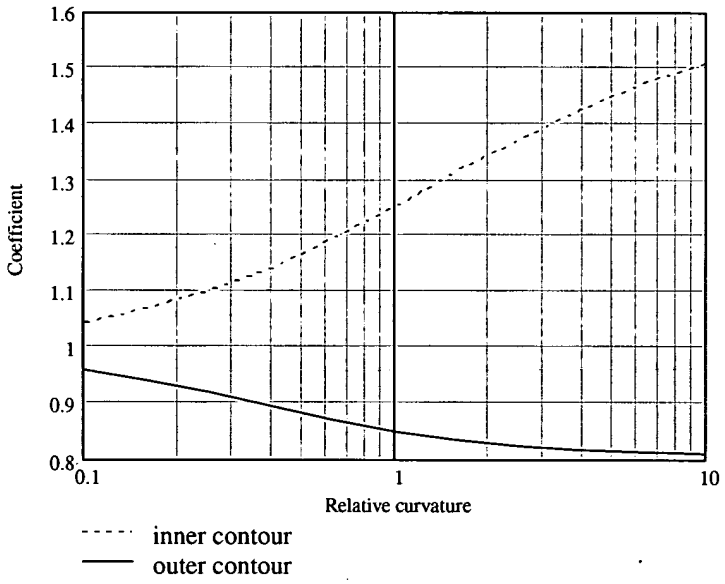

Fig. 21.5. A dependence of the coefficients k_l^i, k_l^o vs. the relative curvature η

As one can see on the plots presented in Fig. 21.5, values of the two other coefficients k_l^i, k_l^o depend essentially on the relative curvature η.

When using the formulae (21.5) and (21.6), one is recommended to take the respective values of the coefficients from the plots given in Fig. 21.5.

21.3. Bi-periodical configurations

The appendix [23] deals with infinitely extensive mattress-like airbags having a bi-periodical system of round adhesive joints. The base for such a bag consists of two infinite sheets of a soft material between which there is a multiple connected hollow. In its working position the hollow contains gas under the pressure p above ambient.

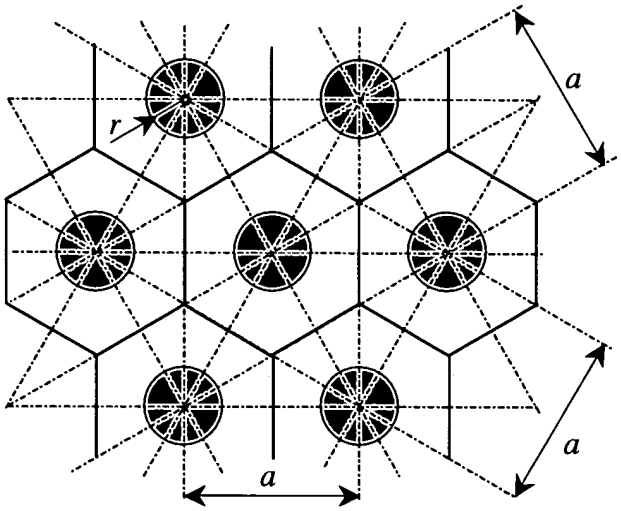

Fig. 21.6. A base for an airbag having a bi-periodical system of round joints placed in nodes of a triangular grid.

Two types of airbags are under consideration. The first one has joints placed in nodes of a triangular grid (Fig. 21.6). The second type has joints placed in nodes of a square grid (Fig. 21.7).

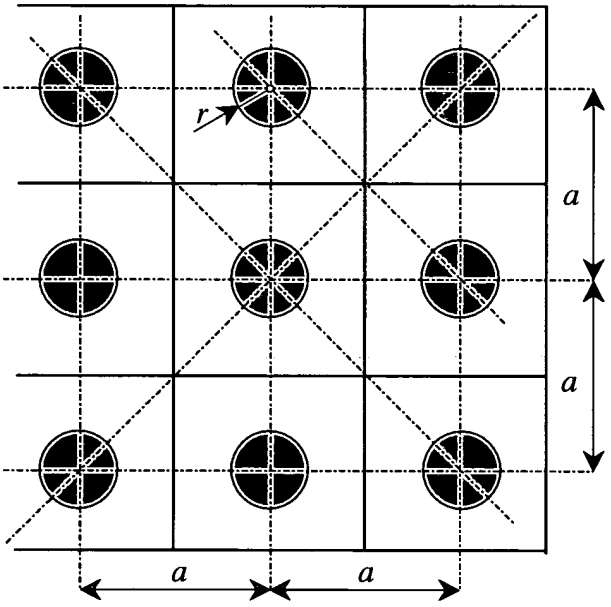

Fig. 21.7. A base for an airbag having a bi-periodical system of round joints placed in nodes of a square grid

In both the first and second case the spacing of the grid is a and the radius of the joint is r.

If we assume the contour of a single joint to be a separate segment of the total contour, then the areas of the infinite plane will be either regular hexagons in the triangular grid case (Fig. 21.6) or squares in the square grid case (Fig. 21.7).

Every area should be divided into sub-areas in order to derive formulae and compare with results of computations presented in [23]. The sub-areas will coincide with elementary cells. Schematics of these sub-areas are shown in Fig. 21.8.

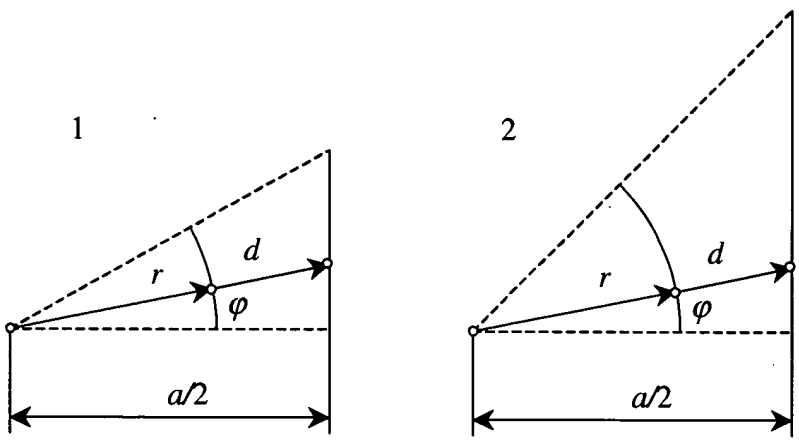

Fig. 21.8. Schematics of sub-areas for the triangular (1) and square (2) grids.

In both cases the distance d from the outline point defined by the angle φ to the boundary of a sub-area is expressed as:

$$d = \frac{a}{2\cos\varphi} - r; \qquad (21.8)$$

and the peeling stress is

$$\psi = k_g k_l p d\left(1 + \frac{d}{2r}\right). \qquad (21.9)$$

The coefficients are found from numerical results of [23].

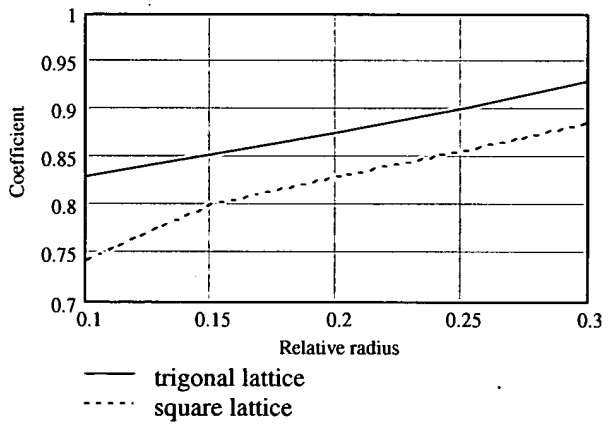

Fig. 21.9. Plots to find the coefficients k_g

Fig. 21.9 shows plots to determine the global coefficients k_g depending on the relative radius of the joint

$$\rho = \frac{r}{a}. \qquad (21.10)$$

The values have been determined from the condition that the sum of all peeling forces found by computing in [23] should be equal to the sum of all peeling forces calculated by the approximate formula (21.9) provided $k_l = 1.0$.

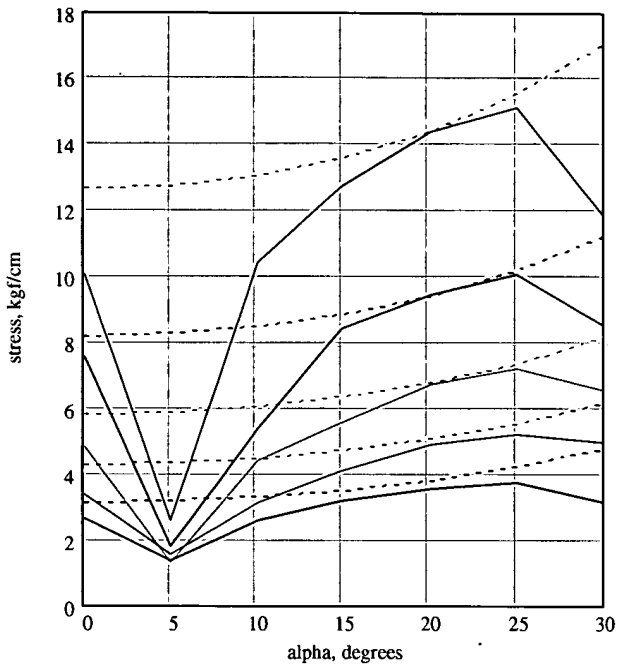

Fig. 21.10. Numerical results (solid lines) majorized by approximate results (dash lines) in the triangular grid case.

As for the distribution of the stress along the circle's contour which is determined essentially by unstable folds, the approximate formula is not capable of describing those. Though, if we assume k_l = 1.27 for the triangular grid, then the approximate curves majorize the numerical results everywhere (see Fig. 21.10).

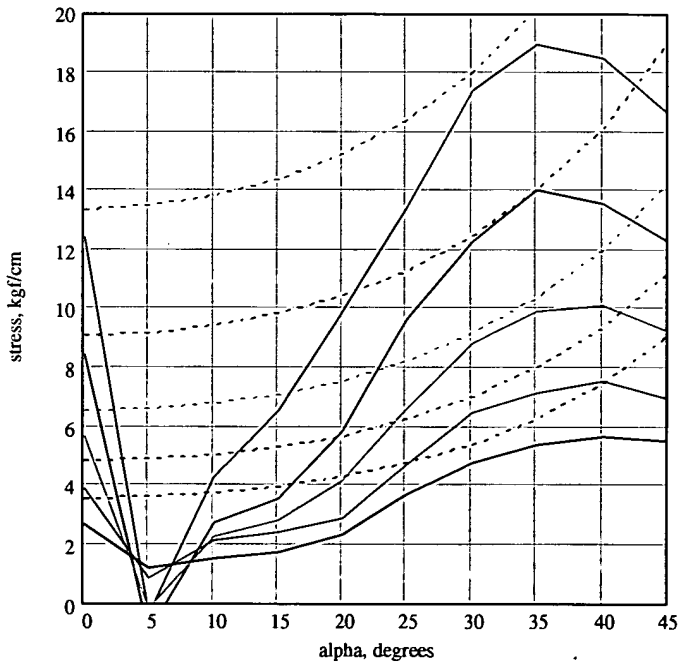

Fig. 21.11. Numerical results (solid lines) majorized by approximate results (dash lines) in the square grid case.

For the square grid one should take k_l = 1.5. Then the approximate curves will majorize the numerical results everywhere, too (see Fig. 21.11).

Five principal curves shown in Fig. 21.10 and Fig. 21.11 present results of solution of five problems different only in the relative radius of the round joint (ρ = 0.1; 0.15; 0.2; 0.25; 0.3).

21.4. Narrow channels

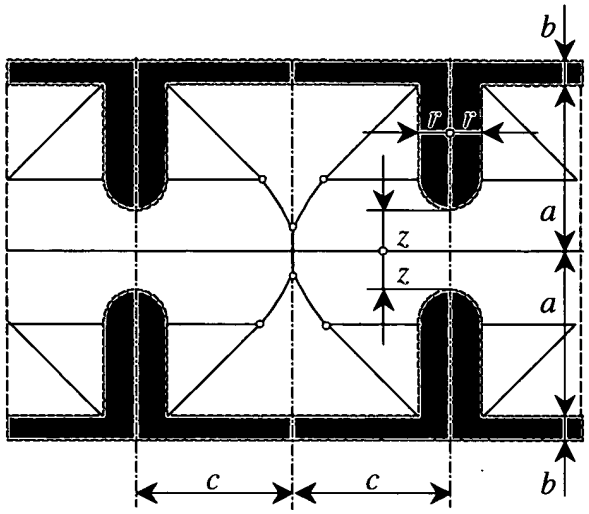

Fig. 21.12. A base for an airbag having narrow channels between adjacent hollows

The appendix [23] presents calculations of the stress/strain distribution in periodic models of airbags that have narrow channels between adjacent hollows. The base for such an airbag consists of two infinite strips of a soft material which form an infinite hollow with narrow necks between them (Fig. 21.12). In its working position it contains gas under the pressure p above ambient.

The same figure shows a division of the region into areas. Due to a symmetry possessed by the system, we can consider only an elementary cell of this system.

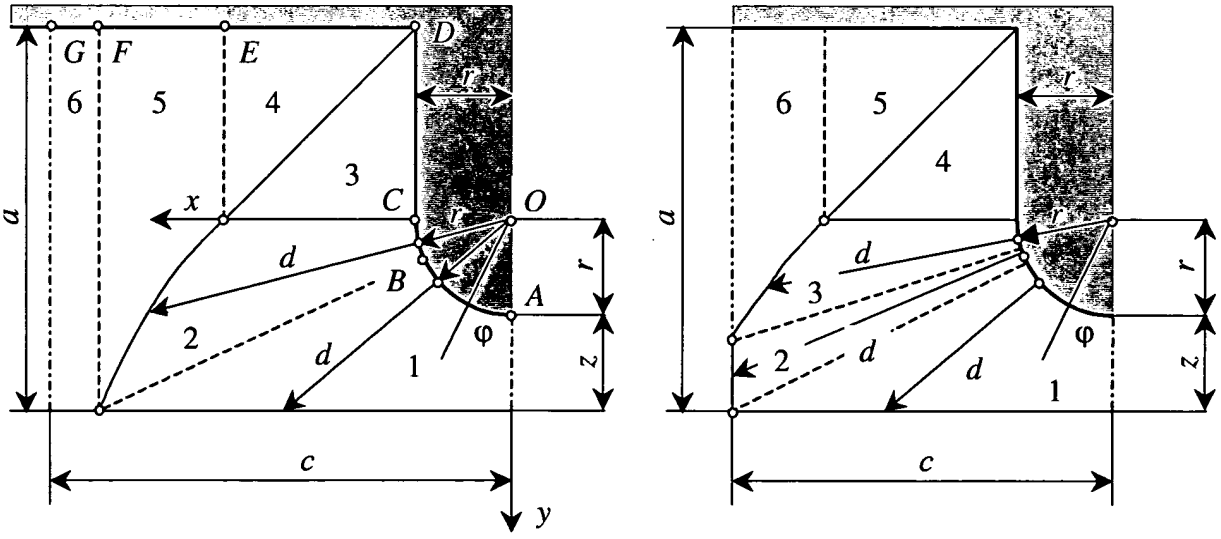

Fig. 21.13. Two options of dividing an elementary cell into areas and sub-areas

Depending on the ratio of sizes, different options of dividing the region into areas and sub-areas can be implemented. Two of them are shown in Fig. 21.13.

Let's discuss an example from the appendix [23] in more detail with the following parameters:

$a = 5$ cm; $c = 9$ cm; $r = 1$ cm; $z = 1$ cm; $p = 1$ kg/cm^2.

In this case a division scheme shown in the left drawing of Fig. 21.13 is implemented. Numbers 1 to 6 denote areas in this drawing. To derive analytical relationships, we use a coordinate system xOy with its origin at the center of the round joint and a polar coordinate system where the angle φ is counted from the axis y. Both systems are shown in Fig. 21.13.

The straight line that bounds the area 1 from below has the following equation in the polar coordinate system:

$$\rho = \frac{z + r}{\cos\varphi}. \qquad (21.11)$$

In the Cartesian coordinate system the equation of this line is

$$y = r + z. \qquad (21.12)$$

The line that divides the areas 2 and 5 is a parabola. The equation of the parabola in the polar coordinate system is:

$$\rho = \frac{a - z}{1 - \cos\varphi}. \qquad (21.13)$$

The same parabola in the Cartesian coordinate system is described by the following equation:

$$y = \frac{a - z}{2}\left(\left(\frac{x}{a - z}\right)^2 - 1\right). \qquad (21.14)$$

Further we will build plots of the peeling stress on the joint's contour. The argument of the plots will be the arc length of the contour s counting from the point A and then passing the points B, C, D, E, F, G.

These points are at boundaries of segments of the joint's contour. Using the drawing and the equations (21.11), (21.14), one can easily write out arc coordinates of these points.

$$s_A = 0; \qquad (21.15)$$

$$s_B = r \cdot \arccos\frac{r + z}{a + r}; \qquad (21.16)$$

$$s_C = \frac{\pi r}{2}; \qquad (21.17)$$

$$s_D = s_0 + r; \qquad (21.18)$$

$$s_E = s_0 + a - z; \qquad (21.19)$$

$$s_F = s_0 + \sqrt{a^2 + 2ar - 2rz - z^2}; \qquad (21.20)$$

$$s_G = s_0 + c; \qquad (21.21)$$

where $s_0 = \frac{\pi r}{2} + a - 2r - z$.

Formulae given below describe the length of the normal for each of the six contour segments.

(21.22) $$d_1 = \frac{r+z}{\cos\frac{s}{r}} - r;$$

(21.23) $$d_2 = \frac{a-z}{1-\cos\frac{s}{r}} - r;$$

(21.24) $$d_3 = s_0 + r - s;$$

(21.25) $$d_4 = s - s_0 - r;$$

(21.26) $$d_5 = \frac{a-z}{2}\left(\left(\frac{s-s_0}{a-z}\right)^2 + 1\right) - r;$$

(21.27) $$d_6 = a.$$

Then, using the formulae (20.5) and (20.6) we can find the peeling stress ψ at each segment.

(21.28) $$\psi_1 = k_g k_l p d_1 \left(1 + \frac{d_1}{2r}\right);$$

(21.29) $$\psi_2 = k_g k_l p d_2 \left(1 + \frac{d_2}{2r}\right);$$

(21.30) $$\psi_i = k_g k_l p d_i \qquad (i = 3..6).$$

The formulae enable us to approximately calculate the peeling stress in the vicinity of the channels between the extended hollows, according to the area division in the left drawing of Fig. 21.13.

Let's compare results obtained by this technique with those obtained by a finite element analysis and presented in the appendix [23]. A example will be a problem with the following geometrical parameters: a = 5 cm; c = 9 cm; r = 1 cm; z = 1 cm at p = 1 kg/cm^2.

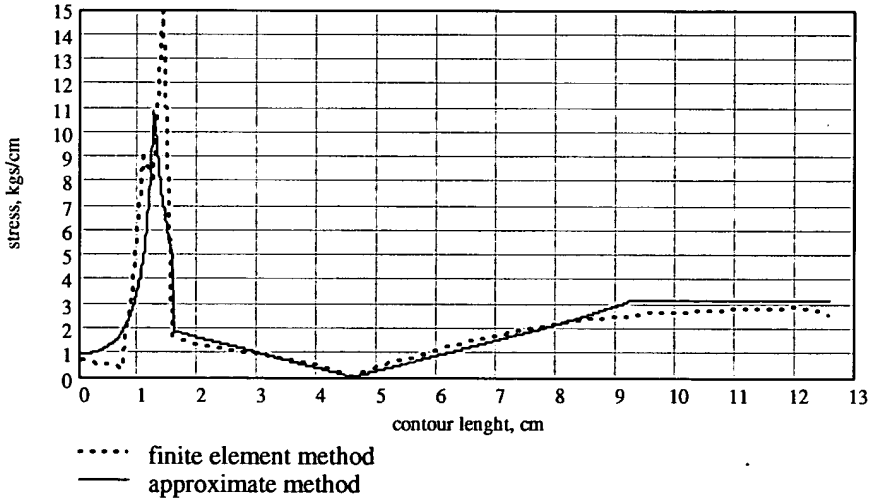

Fig. 21.14. A comparison of results yielded by the approximate method and the finite element analysis.

Fig. 21.14 shows two curves. One of them has been obtained by the finite element analysis using the ANSYS software, and the other one by the technique proposed here. The global correction coefficient k_g has been assumed 0.626 from the condition that the sum of the peeling forces in the approximate solution should be equal to the sum of those in the finite element solution. The local correction coefficients k_l have been assumed equal to one.

The plots show qualitatively matching results. The quantitative correspondence is satisfactory in the area of a smooth stress variation and somewhat worse in places of an intensive stress concentration. In these locations the results can be corrected by introducing appropriate local correction coefficients.

Note that the finite element analysis also yields a substantial spread of results in locations of intensive stress concentration. To find out true values of the peeling stress in these locations, a refined research or an experiment is needed.

22. RESEARCH CAPABILITIES OF THE METHOD

The approximate method is completely determinate and lets one build even analytical relationships, as we did in the previous section. Fig. 22.1 and Fig. 22.2 show plots of these relationships for the problem considered earlier.

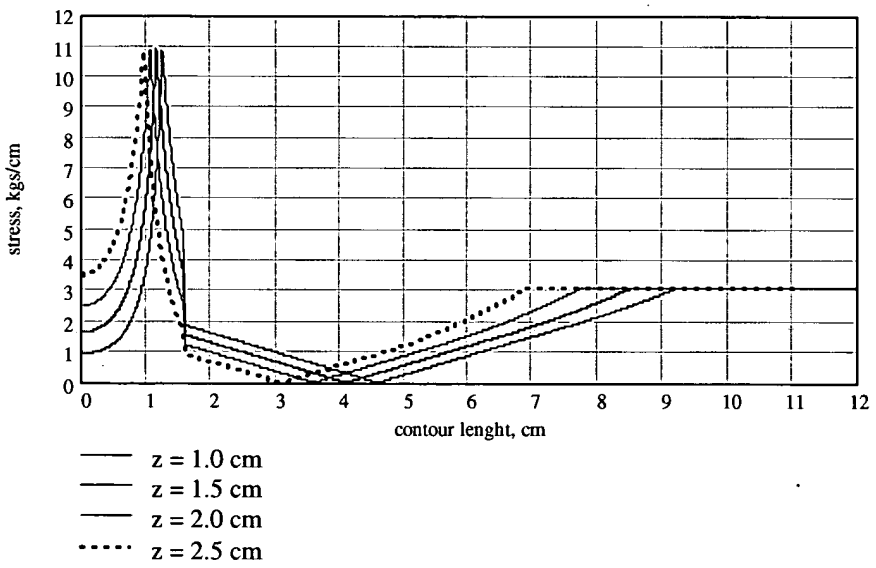

Fig. 22.1. A dependence of the peeling stress vs. the channel's half-width z for the problem illustrated by Fig. 21.12, with the sizes $a = 5$ cm; $b = 0$ cm; $c = 9$ cm; $r = 1$ cm. Parameters $p = 1$ kgf/cm^2; $k_g = 0.626$; $k_l = 1$ are assumed.

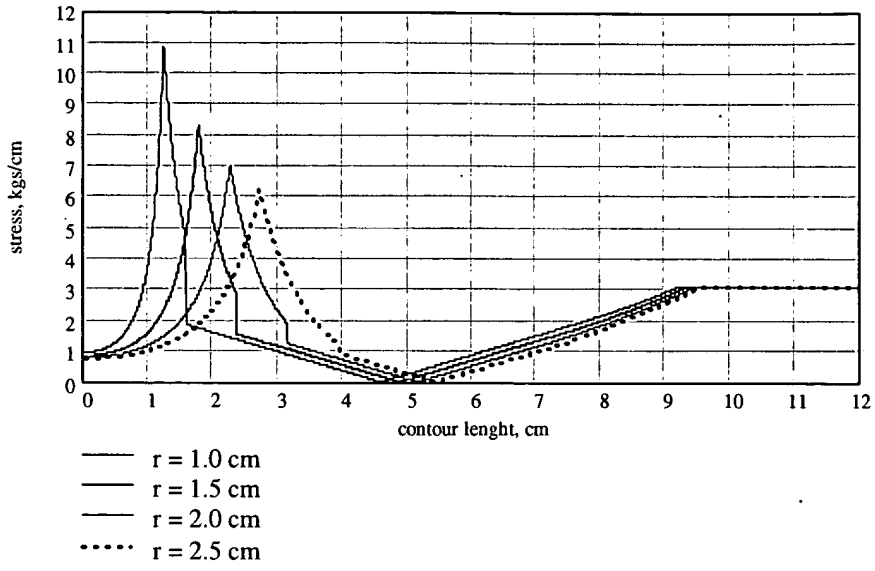

Fig. 22.2. A dependence of the peeling stress vs. the rounded corner radius r for the problem illustrated by Fig. 21.12, with the sizes $a = 5$ cm; $b = 0$ cm; $c = 9$ cm; $z = 1$ cm. Parameters $p = 1$ kg/cm^2; $k_g = 0.626$; $k_l = 1$ are assumed.

When considering Fig. 22.1, we notice that the maximum peeling stress does not depend on the channel width; instead, it depends only on the joint curvature radius. More accurate methods should be employed to check whether it is true.

2. METHOD OF INSCRIBED CIRCLES

In chapter 1 an approximate method intended to calculate the peeling stress in airbags is proposed. This method is quite convenient to build plots of the peeling stress vs. an arc coordinate of a contour.

This chapter presents a method to conveniently determine the peeling stress in a particular point of the contour or to find a maximum stress at a segment of the contour having a constant curvature.

The theory of the method presented here matches that described in the chapter 1 exactly. Therefore both methods yield the same results.

2.1. Inscribed circles

Let a protection airbag, one made of two film sheets glued together, lie on a plane deflated. Let's consider an area where the film sheets are not joined between each other. We assume that the adhesive joint's contour, that is its boundary, belongs to the area itself too. Then, we place a circle inside the area and start increasing its radius, only trying to keep all its points within the area. A circle the radius of which cannot be increased any more, will be referred to as a circle inscribed in the area.

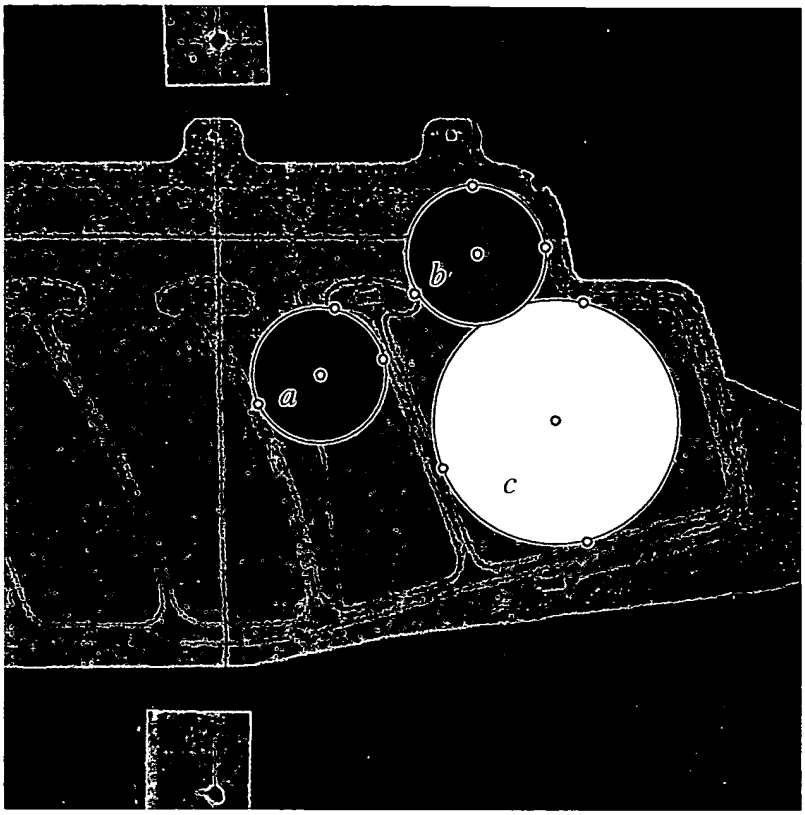

Fig. 2.1. Examples of circles inscribed in areas where the sheets are not glued together

Fig. 2.1 shows a fragment of a protection airbag for the "Saturn" car and examples of circles inscribed in areas where the sheets that make the airbag are not glued between each other. One may notice each circle touches its area's boundary at three points. These points are ringed. So are the centers of the inscribed circles.

There may be cases (Fig. 2.2) when an inscribed circle touches its area's boundary at two points only. Also, one can imagine cases when an inscribed circle touches its area's boundary at more than three points, up to an infinite number thereof, for example, if a round area is under consideration. Though, there can be no circle that touches its area's boundary at one point only.

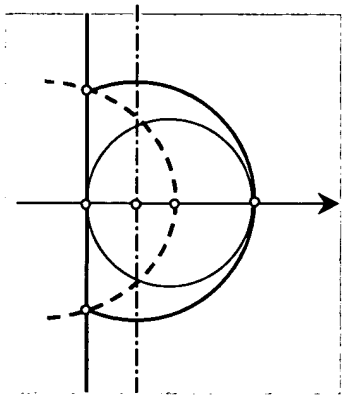

Fig. 2.2. An example of an inscribed circle with two tangency points

If the position of a circle inside an area has been subjected to additional constraints/limitations of any kind, and then its radius has been increased until it cannot grow anymore, such circle will be referred to as conditionally inscribed in the area.

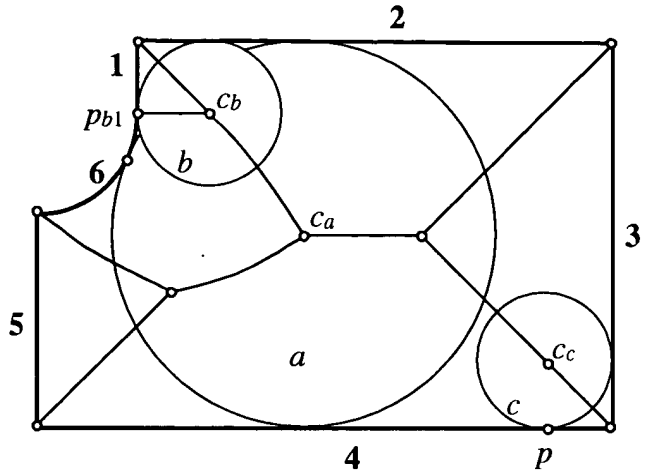

Fig. 2.3. Conditionally inscribed circles. *a* – when the tangency to the segment 6 is required; *b* – when the tangency to the segment 1 is required; *c* - when the tangency at the point *p* is required

Fig. 2.3 shows an example of an area from chapter 1 where three conditionally inscribed circles are presented. The *a* circle is inscribed in the area and required to touch the segment 6 of its boundary. Its diameter cannot be increased any more because the area's boundary segments 2 and 4 do not allow it. The *b* circle is inscribed in the area and required to touch the segment 1 of its boundary. The diameter of it cannot be increased being bounded by the segment 2 and due to the fact that the point p_{b1} of tangency between the circle b and the segment 1 may not leave the segment. The circle *c* is inscribed in the area and required to touch the segment 4 of the area's boundary at a fixed point *p*. Its diameter is limited by the presence of the segment 3 of the boundary.

Inscribed circles and those conditionally inscribed can be plotted easily on a computer the display of which shows the outline of the adhesive joint between the sheets of an airbag. One can use a program such as Microsoft Graph that provides one with the option to plot and move around circles with their diameters specified by numbers.

2.2. Locus of centers of inscribed circles

Returning to the chapter 1, let's recall that the adhesive joint's contour that is the boundary of the area in question can be divided into a finite or infinite number of segments on the basis of any conceivable considerations. The area of interest can be divided into sub-areas so that each segment of the boundary correspond to a particular sub-area. The sub-area that corresponds to a segment should consist of points to which this particular segment is nearest. If a point is equidistant from two segments of the area's boundary, it is assumed to belong to the boundary between the sub-areas that conform to these two segments. A segment of the boundary between two sub-areas can be defined as a locus of points equidistant from two appropriate segments of the adhesive joint's boundary.

If an inscribed circle touches two segments of the area's boundary, then its center is equidistant from these segments. If we build a conditionally inscribed circle tangential to a particular segment of the boundary at a fixed point, then it will touch some other segment of the boundary in the general case.

Thus, the locus of centers of conditionally inscribed circles required to touch a fixed point of a particular segment of the area's boundary is the boundary of the sub-area that conforms to this segment (see the circle *c* in Fig. 2.3).

The center of a conditionally inscribed circle that touches a particular segment is a point of the area farthest from this segment. Generally, it is located exactly where boundaries of three segments cross one another (see the *a* circle in Fig. 2.3).

The center of an inscribed circle is a point farthest from boundaries of an area. This maximum should be treated as a local one. This can be confirmed by the example given in Fig. 2.1.

2.3. Application of the method of inscribed circles

It can be seen that the peeling stress can be calculated using inscribed circles and the main formula (20.5).

The method of inscribed circles is convenient for the solution of three types of problems.

2.3.1. Determining the peeling stress in a given point of the joint's contour.

To solve this problem one should plot an inscribed circle that must touch the contour in the given point (see the *c* circle in Fig. 2.3) and measure its radius *d*.

Next, one should use the formula (20.5).

We assume that the radius of curvature *r* of the contour in the given point is known.

2.3.2. Calculating the maximum peeling stress at a segment of a contour of a constant curvature.

To solve this problem, one should build an inscribed circle required to touch the contour's segment in question (see the *a* and *b* circles in Fig. 2.3) and measure its radius *d*.

Next, one should use the formula (20.5).

We assume that the radius of curvature *r* of the contour's segment in question is known.

The point where the inscribed circle touches the contour is exactly the one where the peeling stress achieves its maximum at this segment.

2.3.3. Finding points of local maximum of the peeling stress at the adhesive joint's contour.

To solve this problem one should build inscribed circles in different areas of the inflatable hollow (see Fig. 2.1). Points where the circles touch the boundary are points of local maximums of the peeling stress at the joint's contour.

One of these points may be a point of the absolute maximum of the peeling stress.

13. APPROXIMATE ANALYSIS OF SIDE AIRBAG FOR "SATURN" CAR

13.1. Formulae for the analysis

The peeling stress is to be determined by the formula (20.5).

The stress in the material is to be determined by the formula:

$$(13.1) \qquad \sigma = \frac{\Psi}{\delta};$$

where δ is the thickness of the material the airbag is made of.

13.2. Source data

The geometrical sizes have been obtained by a photogrammetry of the side curtain airbag intended for a "Saturn" car (see Fig. 13.1 and Fig. 13.2). The thickness of the material the airbag is made of is δ = 0.015 cm. The elasticity modulus of the material is not used. The technique applied here does not take it into account considering the material to be inextensible. The pressure is assumed to be p = 0.5 kg/cm^2. The global coefficient is k_g = 0.64.

The analysis was performed for 15 characteristic points of the airbag denoted by circles and numbered in Fig. 13.1 and Fig. 13.2. Values of *d* and *r* for these points have been measured on the picture and are given in a table of data below. The local coefficients k_l have been adopted on the basis of practical experience. These are presented in the table, too.

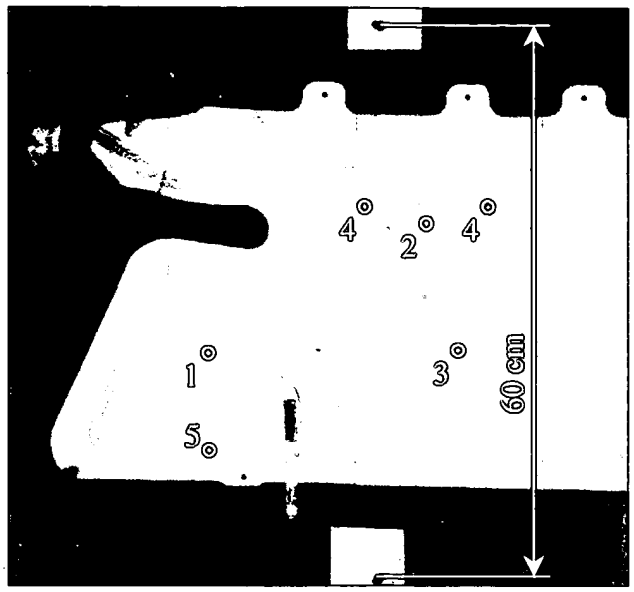

Fig. 13.1. Locations of points 1..5 where the stress in the material and the peeling stress in the adhesive joint have been determined

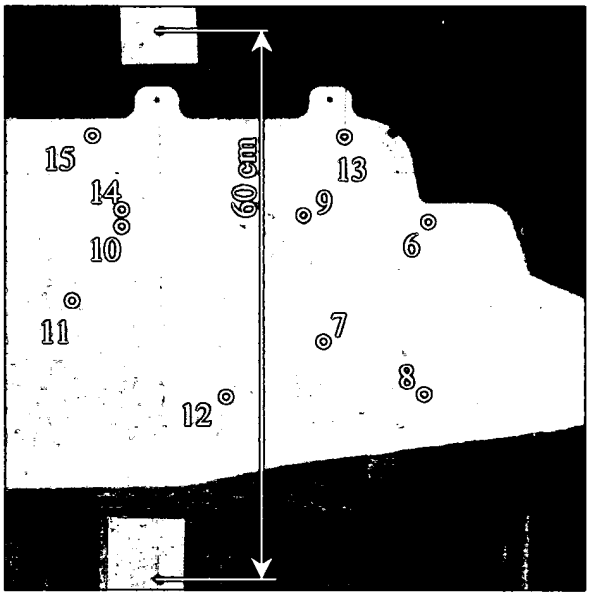

Fig. 13.2. Locations of Points 6..15 where the stress in the material and the peeling stress in the adhesive joint have been determined

22.1. Results of the analysis

The source data relating to the points and results of the analysis performed are presented in the table below.

No of point	d cm	r cm	k_l	ψ kg/cm	σ kg/cm^2
1	6.0	1.0	1.4	10.752	716
2	5.5	1.0	1.4	9.240	616
3	5.5	∞	1.0	1.760	117

No of point	d cm	r cm	k_l	ψ kg/cm	σ kg/cm^2
4	4.8	1.0	1.4	7.311	487
5	6.0	∞	1.0	1.920	128
6	9.8	4.2	1.2	8.154	543
7	9.8	∞	1.0	3.136	209
8	9.8	120.0	1.0	3.264	217
9	5.7	1.0	1.4	9.831	655
10	5.4	1.0	1.4	8.951	596
11	5.4	80.0	1.0	1.786	119
12	5.5	40.0	1.0	1.881	125
13	5.7	∞	1.0	1.824	121
14	4.8	1.0	1.4	7.311	487
15	4.8	∞	1.0	1.536	102

According to the tentative data, the greatest stress appears in the vicinity of Point 1. It can be reduced by increasing the radius of the adhesive joint near this point. The stress in Points 6 and 9 can be reduced by narrowing the hollow between Points 6, 7, 8, 9. The stress in Points 2, 10, 14 and other similar ones can be reduced by altering the shape of the bulb-like ends of the adhesive joints.

3. IMPROVEMENT OF APPROXIMATE METHOD

A comparison of results yielded by the approximate method and the finite element analysis shows that the former gives the lower peeling stress in locations where the adhesive joints have small radii of rounding. We suggest that the main formula of the approximate method be modified in order to reduce the said error.

The basis for this modification will be an axisymmetric analysis of stresses at the boundary of an annular hollow [23]. The idea is that the new formula should yield accurate results for both cylindrical and annular hollows.

3.1. Analysis of stresses near an annular hollow in an airbag made of inextensible material

The appendix [23] gives a numerical analysis of an annular hollow in elastic material. This section presents an attempt to solve the same problem in a closed form for the case of a soft inextensible material, in order to find proper analytical relationships.

The object of consideration is an airbag made of two round pieces of film with the radius b, glued together along their exterior contours and in the interior of a circle at the central parts thereof that has the radius a. The drawing of it is presented in Fig. 1.1. The airbag has an annular hollow with its width in the initial state $b - a$. When the airbag is inflated, its exterior radius decreases and becomes R at the end of the inflation process.

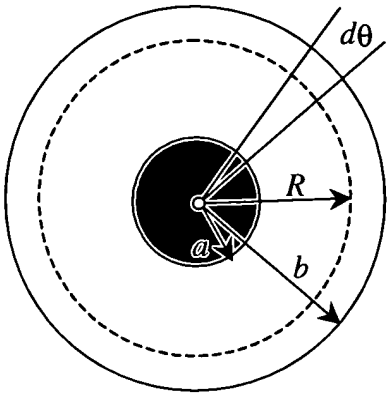

Fig. 3.1. An airbag having an annular hollow.

The thickness of the film is small, the film material is inextensible but easily foldable. We assume that folds are "spread" evenly.

The problem is how to describe the deformed state of the bag and find the peeling stress in the adhesive joint when the hollow is filled with gas at a pressure p above ambient.

As the airbag is a body of revolution, its shape is unambiguously defined by a fragment of a curve being a meridional section of the bag's shell. This curve is shown in Fig. 3.2.

Because all points of the hollow decrease their coordinates x when the airbag is inflated, all annular fibers will be unstressed. The annular stress will be zero in the hollow area. Only the radial stress will be present.

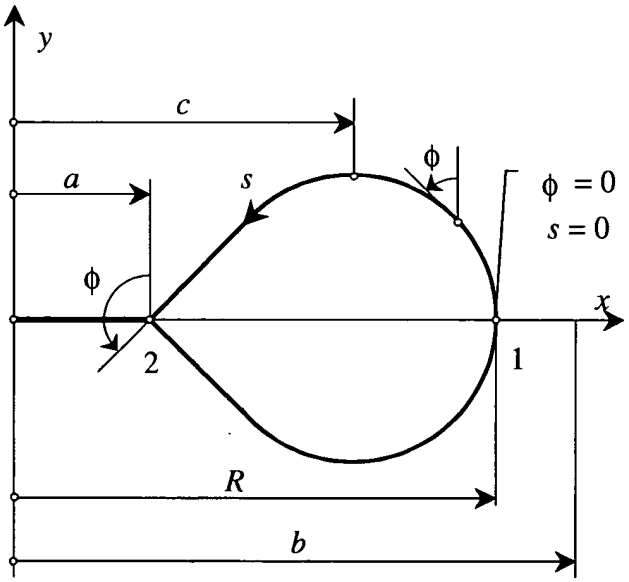

Fig. 3.2. A radial section

We assume that the meridional section is specified by the coordinates x and y parametrically vs. the meridian arc length s.

To shorten the notation, let's designate the derivatives with respect to arc length by a stroke:

$$(3.1) \qquad x' = \frac{dx}{ds};\ x'' = \frac{d^2x}{ds^2};\ y' = \frac{dy}{ds};\ y'' = \frac{d^2y}{ds^2}.$$

With this notation introduced, the meridian curvature will be described by the formula:

$$(3.2) \qquad \kappa = x' \cdot y'' - y' \cdot x''$$

Having extracted a sector with the opening angle $d\theta$ (see Fig. 1.1), we can write the equation of equilibrium of a soft shell strip located in this sector, in this way:

(3.3) $$H \cdot \kappa \cdot d\theta = p \cdot x \cdot d\theta ;$$

where H designates the internal radial stress in the bag's material per one radian of the angular coordinate θ.

After the reduction and substitution of the variable κ from the equation (3.2), we have:

(3.4) $$H(x' \cdot y'' - y' \cdot x'') = p \cdot x .$$

As

(3.5) $$x'^2 + y'^2 = 1 ;$$

we can change the variables in this way:

(3.6) $$x' = -\sin\phi ;$$

(3.7) $$y' = \cos\phi .$$

The angle ϕ has the geometrical sense according to Fig. 3.2.

After this substitution of variables the second derivatives of the coordinates x and y can be expressed by these formulae:

(3.8) $$x'' = \sin\phi \cdot \cos\phi \cdot \frac{d\phi}{dx} ;$$

(3.9) $$y'' = \sin^2\phi \cdot \frac{d\phi}{dx} .$$

Substituting the derivative expressions of the formulae (3.6) - (3.9) to the formula (3.4) will give us this:

(3.10) $$H(-\sin\phi \cdot \sin^2\phi - \cos^2\phi \cdot \sin\phi)\frac{d\phi}{dx} = p \cdot x .$$

The result is a differential equation with variables separable:

(3.11) $$-\frac{H}{p}\sin\phi \cdot d\phi = x \cdot dx .$$

Solution of this equation in quadratures at the initial conditions $x = R$, $\phi = 0$ gives this result:

(3.12) $$-\frac{H}{p}\int_0^{\phi} \sin\phi \cdot d\phi = \int_R^{x} x \cdot dx ;$$

(3.13) $$-\frac{H}{p}(1-\cos\phi) = \frac{x^2}{2} - \frac{R^2}{2} .$$

The relationship of the coordinate x vs. the angle ϕ can be easily found in a closed form from the above expressions:

(3.14) $$x = \sqrt{R^2 - \frac{2H}{p}(1-\cos\phi)} .$$

Introducing dimensionless values ξ and γ according to the formulae:

(3.15) $$\xi = \frac{x}{R}$$

(3.16) $$\gamma^2 = \frac{H}{pR^2}$$

will give us

(3.17) $$\xi = \sqrt{1 - 2\gamma^2(1 - \cos\phi)}\,.$$

The physical meaning of ξ is a dimensionless radial coordinate.
The same formula can be presented in a different form:

(3.18) $$\xi = \sqrt{1 - \left(2\gamma \sin\frac{\phi}{2}\right)^2}\,.$$

Having introduced a value

(3.19) $$u = 2\sin\frac{\phi}{2};$$

we can write:

(3.20) $$\xi = \sqrt{1 - (\gamma u)^2}\,.$$

Now we have to determine the coordinate y and the arc length s versus the angle ϕ (see Fig. 3.2). For this purpose we use the formula:

(3.21) $$\frac{dx}{d\phi} = \frac{dx}{ds}\frac{ds}{d\phi}.$$

Substituting the derivatives $\frac{dx}{ds}$ и $\frac{dx}{d\phi}$ taken from the formulae (3.6) and (3.14) in here will give:

(3.22) $$\frac{ds}{d\phi} = \frac{H}{px}.$$

Another relationship can be introduced:

(3.23) $$\frac{dy}{d\phi} = \frac{dy}{ds}\frac{ds}{d\phi}.$$

This relationship together with the formulae (3.7) and (3.22) yields:

(3.24) $$\frac{dy}{d\phi} = \frac{H\cos\phi}{px}.$$

Next, we pass to dimensionless variables:

(3.25) $$\sigma = \frac{s}{R};$$

(3.26) $$\eta = \frac{y}{R};$$

and perform some simple transformations to derive this:

$$(3.27)\qquad \frac{d\sigma}{d\phi}=\frac{\gamma^2}{\xi};$$

$$(3.28)\qquad \frac{d\eta}{d\phi}=\frac{\gamma^2}{\xi}-\frac{(\gamma u)^2}{2\xi}.$$

Thus, the dimensionless arc length σ and the dimensionless ordinate η can be described by these quadrature formulae:

$$(3.29)\qquad \sigma=\gamma^2\int_0^{\phi}\frac{d\phi}{\xi};$$

$$(3.30)\qquad \eta=\frac{\gamma^2}{2}\int_0^{\phi}\frac{2-u^2}{\xi}d\phi.$$

The functions σ and η can be expressed via elliptic integrals of the first and second kind:

$$(3.31)\qquad \sigma=2\gamma^2\cdot F\left(2\gamma,\frac{\phi}{2}\right)$$

$$(3.32)\qquad \eta=(2\gamma^2-1)F\left(2\gamma,\frac{\phi}{2}\right)+E\left(2\gamma,\frac{\phi}{2}\right)$$

Recall that the elliptic integral of the first kind is

$$(3.33)\qquad F(k,\varphi)=\int_0^{\varphi}\frac{d\theta}{\sqrt{1-k^2\cdot\sin^2\theta}};$$

and the elliptic integral of the second kind is

$$(3.34)\qquad E(k,\varphi)=\int_0^{\varphi}\sqrt{1-k^2\cdot\sin^2\theta}\cdot d\theta.$$

The elliptic integrals are built-in functions in many mathematical software programs where they are tabulated.

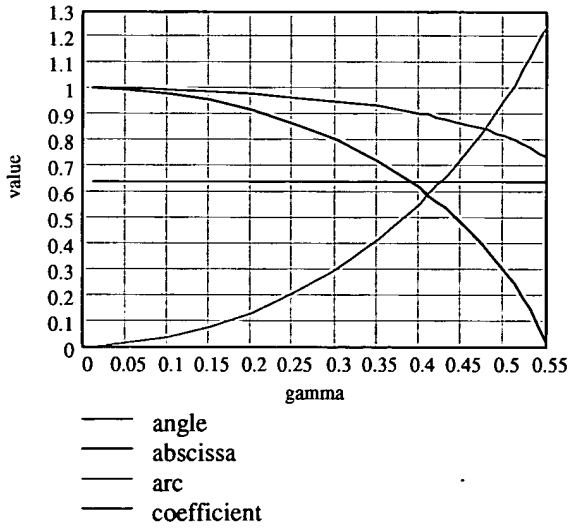

Fig. 3.3. Dimensionless values to describe the shape of the hollow

Fig. 3.3 presents plots of dimensionless parameters that describe the hollow shape vs. the value of γ:

angle - the relative value of ϕ/π at the point 2;

abscissa - the value of ξ at the point 2;

arc - the value of σ at the point 2;

coefficient - the value of the global coefficient $k_g = \dfrac{R^2 - a^2}{b^2 - a^2}$.

Numbers of the points and designations of the values are shown in Fig. 3.2.

It is pretty unexpected to see such a stable behavior of the global coefficient k_g. It is little dependent on the parameter γ. This result can be used to derive approximate formulae.

3.2. Peeling stress

Above we used the following formula to determine the peeling stress approximately:

$$\psi = k_g k_l p d\left(1 + \frac{d}{2r}\right); \qquad (3.35)$$

where p is the internal pressure above ambient;

d is the inscribed circle radius (see Fig. 20.1);

r is the curvature radius of the joint's contour (positive if the convexity of the contour looks inwards the hollow, and negative otherwise);

k_g is a global coefficient to take into account how much the area of the horizontal projection of the airbag's hollow filled with air is less than the hollow's area in the flat airbag;

k_l is a local coefficient to take into account deviations of the actual stress from its approximate values in local areas of the airbag.

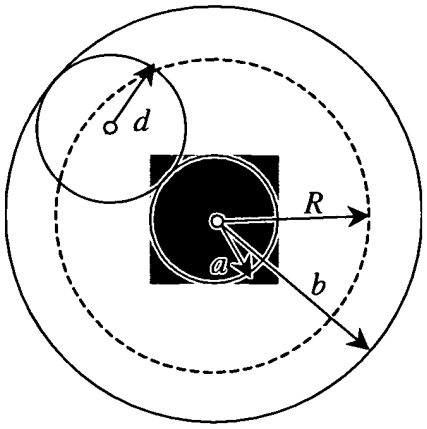

Fig. 3.4. To the determination of the peeling stress

The experience of using this formula has shown the correction coefficients k_g and k_l to be too much variable and undesirably different from one. While the coefficient k_g usually equals 0.6 to 0.7, the coefficient k_l in locations of small radii (with respect to d) of the contour's rounded corners reaches as high as 2 or even more.

Therefore this report presents an attempt to replace that formula with a better one by introducing the global coefficient $\frac{2}{\pi}$ directly into the formula. This value is true for cylindrical and annular hollows [23], so we have just to make such corrections as to make the formula almost match the exact solutions for these cases.

The structure of the new formula is this:

$$\psi = c_g c_l \frac{2pd}{\pi} f(\eta). \qquad (3.36)$$

It keeps a global coefficient (one and the same for the whole problem being solved) c_g and a local coefficient c_l. But these are different coefficients from those in (3.35).

The formula contains a functions $f(\eta)$ still undefined, where

$$\eta = \frac{d}{r}. \qquad (3.37)$$

To find the value, we use the solution for the annular hollow in an inextensible airbag obtained in the previous section.

These results can be used to determine the peeling stress at the exterior and interior contours of the adhesive joint.

The stress at the exterior contour is described by the formula:

$$\psi_1 = \frac{H}{b} = \frac{\gamma^2 pR}{\xi_2 + \sigma_2}. \qquad (3.38)$$

The stress at the interior contour is described by the formula:

$$\psi_2 = -\frac{H\cos\phi_2}{a} = -\frac{\gamma^2 pR\cos\phi_2}{\xi_2}. \qquad (3.39)$$

In these and further formulae the subscript 1 designates values referring to the exterior contour, while the subscript 2 designates quantities belonging to the interior contour.

Assuming the correction coefficients in the formula (3.36) to equal one, we equate values of the peeling stress obtained by this formula with their values in the formulae (3.38) and (3.39). These equalities can be used to find the functions $f(\eta)$ for both cases.

The first of the equalities is

$$\frac{2pd}{\pi} f_1(\eta_1) = \frac{\gamma^2 pR}{\xi_2 + \sigma_2}. \qquad (3.40)$$

Seeing that

$$d = \frac{\sigma_2 R}{2}; \qquad (3.41)$$

we can derive the formula to find $f_1(\eta_1)$:

$$f_1(\eta_1) = \frac{\pi\gamma^2}{\sigma_2(\sigma_2 + \xi_2)}. \qquad (3.42)$$

One should consider that

$$(3.43) \qquad \eta_1 = -\frac{\sigma_2}{2(\sigma_2 + \xi_2)}.$$

It should be noted that in the solution presented in Section 3.1 all values are functions of the parameter γ. Thus the formulae (3.42), (3.43) express the functional relationship $f_1(\eta_1)$ parametrically.

In the same way we obtain this:

$$(3.44) \qquad f_2(\eta_2) = -\frac{\pi\gamma^2 \cos\phi_2}{\sigma_2 \xi_2};$$

$$(3.45) \qquad \eta_2 = \frac{\sigma_2}{2\xi_2}.$$

The functional relationships $f_1(\eta_1)$ and $f_2(\eta_2)$ are presented as plots in Fig. 3.5 and Fig. 3.6.

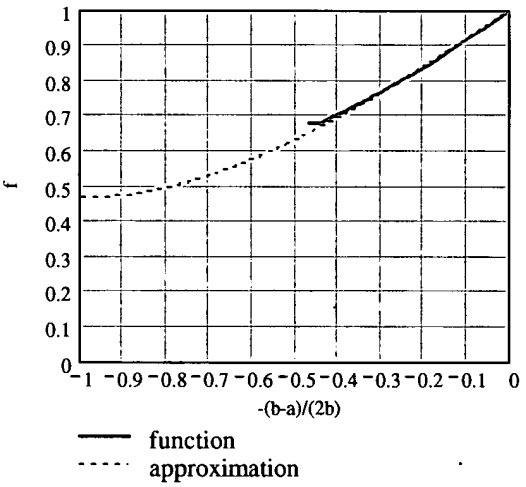

Fig. 3.5. Plot of the functional relationship $f_1(\eta_1)$ for the exterior contour

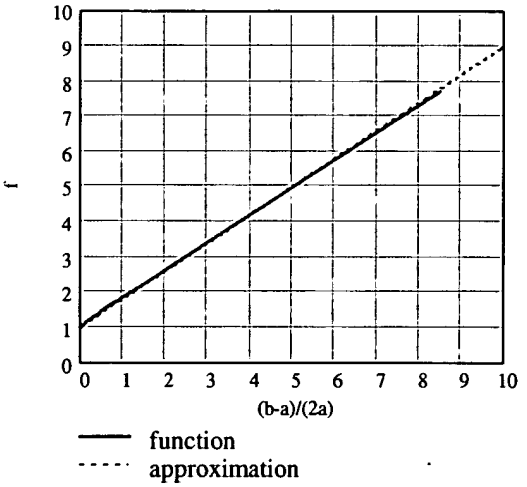

Fig. 3.6. Plot of the functional relationship $f_2(\eta_2)$ for the interior contour

These approximating formulae are adopted:

(3.46) $$f_1(\eta_1) = 1 + 0.8\eta_1 + \frac{0.8}{3}\eta_1^2;$$

(3.47) $$f_2(\eta_2) = 1 + 0.8\eta_2.$$

Fig. 3.5 and Fig. 3.6 show plots of these functions as dash lines.

The approximating formula (3.46) is built in such way that it gives a correct result also for the driver's airbag made of two round film pieces glued together.

3.3. New formulae

Thus, when making use of the approximate methods described in the chapters 1 and 3, one is recommended to adhere to the same methodology but employ these new analytic formulae:

(3.48) $$\psi = c_g c_l \frac{2pd}{\pi}(1 + 0.8\eta)$$ - for convex parts of the contour;

(3.49) $$\psi = c_g c_l \frac{2pd}{\pi}$$ - for straight parts of the contour;

(3.50) $$\psi = c_g c_l \frac{2pd}{\pi}(1 + 0.8\eta + \frac{0.8}{3}\eta^3)$$ - for concave parts of the contour;

(3.51) $$\eta = \frac{d}{r}.$$

Here p is the internal pressure above ambient inside the airbag's hollow;

d is the radius of the inscribed circle;

r is the curvature radius of the joint's contour (positive if the convexity of the contour looks inwards the hollow, negative otherwise);

c_g is a global coefficient to take into account a deviation of the actual stress from its approximate values, being the same for the whole analysis;

c_l is a local coefficient to take into account deviations of the actual stress from its approximate values in the local area of the contour.

The coefficients c_g and c_l are determined by comparing results yielded by the approximate method with either results of more accurate techniques or experimental data. If there are none of both, the coefficients are assumed to equal 1.

22.2. Comparison of results

The object of consideration is the side head protector airbag for the "Saturn" car that has been already analyzed before.

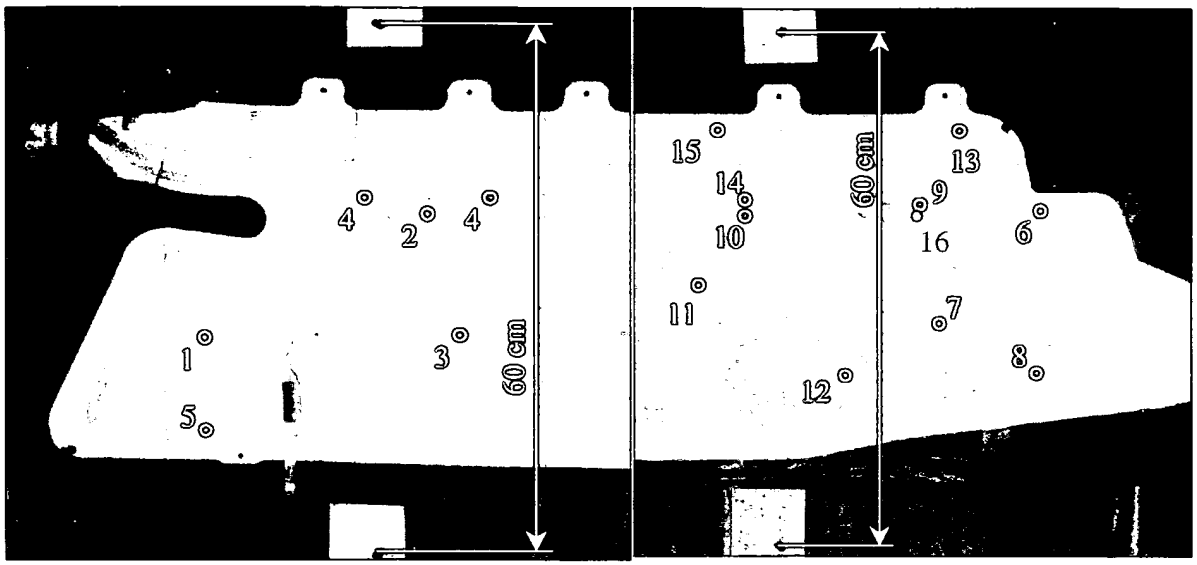

Fig. 3.7. Cap areas of the side head protector airbag for the "Saturn" car, with points numbered

Table 13 and Table 14 list results obtained by the approximate method using the old formulae from chapter 13, by the approximate method using the new formulae, and by the finite element analysis.

Table 13. Stress values at the boundary of the hollow nearest to the inlet.

N of point	d cm	r cm	k_l	ψ kg/cm	ψ_n kg/cm	ψ_e kg/cm
1	6.0	1.0	1.4	10.752	11.077	18.00
2	5.5	1.0	1.4	9.240	9.454	10.40
3	5.5	∞	1.0	1.760	1.751	1.75
4	4.8	1.0	1.4	7.311	7.395	7.20
5	6.0	∞	1.0	1.920	1.910	1.85

Table 14. Stress values at the boundary of the hollow remotest from the inlet.

N of point	d cm	r cm	k_l	ψ kg/cm	ψ_n kg/cm	ψ_e kg/cm
6	9.8	4.2	1.2	8.154	8.942	7.09
7	9.8	∞	1.0	3.136	3.119	2.72
8	9.8	120.0	1.0	3.264	3.323	2.84
9	5.7	1.0	1.4	9.831	10.088	8.55
13	5.7	∞	1.0	1.824	1.814	1.60
16	7.48	1.0	1.4	15.884	16.629	15.95

These designations are used in the tables:

d is the radius of the inscribed circle;

r is the curvature radius of the contour;

ψ are the stresses calculated by the approximate method using the old formula (3.35). It is assumed that $k_g = 0.64$ and k_l is different at different points according to the tables.

ψn are the stresses obtained by the approximate method using new formulae. It is assumed that $c_g = c_l = 1$.

ψe are the stresses calculated by the finite element method.

As the comparison shows, results obtained with the new formulae are generally better than those obtained with the old formulae. Both are generally close to the results of the finite element analysis. Though, it should be noted that the values of ψn have been found at $c_g = c_l = 1$ and can be improved additionally by varying these coefficients.

14. APPROXIMATE ANALYSIS OF IMPROVED SIDE AIRBAG FOR "SATURN" CAR

На базе расчетов, приведенных в главе 13, был сделан вывод о целесообразности совершенствования боковой подушки безопасности для автомобиля "Сатурн". The goal of the improvement was to reduce the peeling stress intensity by changing the shape of adhesive joints between sheets that make up the airbag.

This chapter presents results of an approximate analysis of the peeling stress in characteristic points of the adhesive joint's contour.

The technique used for this analysis has been presented in chapters 2 and 3.

14.1. Formulae for calculation

The peeling stress is calculated by the following formulae:

(14.1) $\psi = c_g c_l \frac{2pd}{\pi}(1 + 0.8\eta)$ at convex segments of the contour;

(14.2) $\psi = c_g c_l \frac{2pd}{\pi}$ at linear segments of the contour;

(14.3) $\psi = c_g c_l \frac{2pd}{\pi}(1 + 0.8\eta + \frac{0.8}{3}\eta^3)$ at concave segments of the contour;

(14.4) $\eta = \frac{d}{r}$.

Here p is an internal pressure above ambient inside the airbag;

d is the radius of an inscribed circle;

r is the radius of curvature of the joint's contour (it is positive if the convexity of the contour looks inwards, or negative if outwards);

c_g is a global coefficient to allow for deviations of the actual stress from its approximate calculated values; this one is uniform in all areas;

c_l is a local coefficient to allow for deviations of the actual stress from its approximate calculated values in a local area of the contour.

14.2. Source data

Geometrical sizes were taken from drawings of improved side airbag for "Saturn" car. The calculation was performed at 45 characteristic points of the airbag which are shown as circles and numbered in Fig. 13.1 and Fig. 13.2. Values of d and r at these points were measured in the drawing. These are presented in the table below. Exceptions are values of r for curvilinear segments obtained by solving appropriate differential equations. In these exceptional cases, theoretically obtained values of the radii were used.

The calculation was performed at p = 0.5 kg/cm^2. The global coefficient was c_g = 1.0. The local coefficients k_l were based on earlier experience.

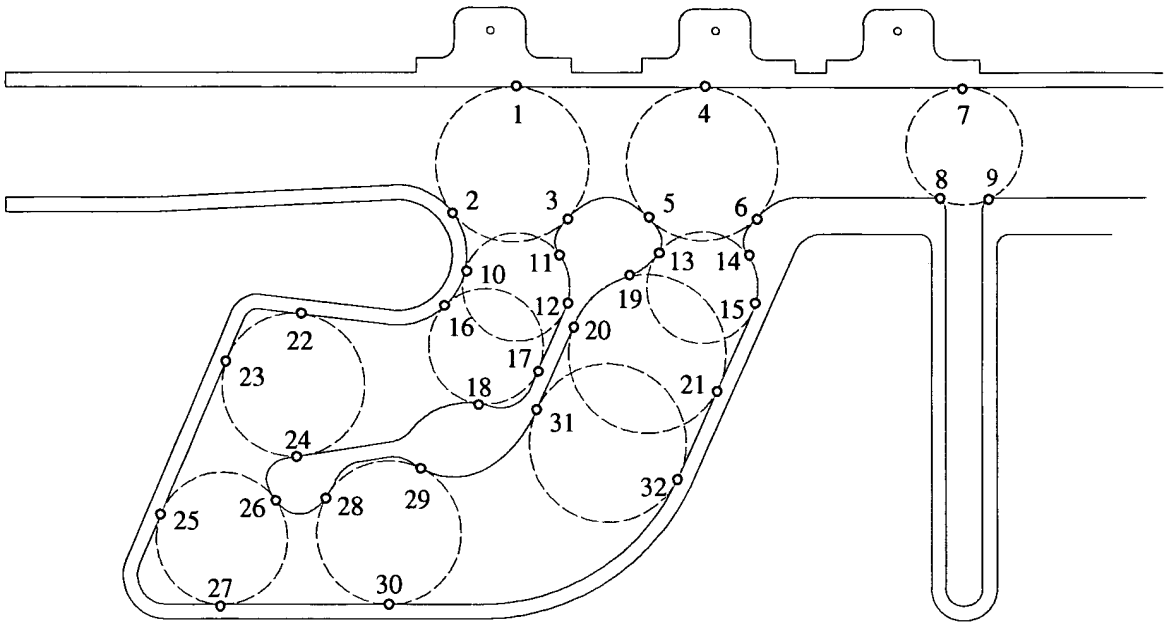

Fig. 14.1. Locations of points 1..32 where the peeling stress values have been determined in the adhesive joint that belongs to the left part of the airbag

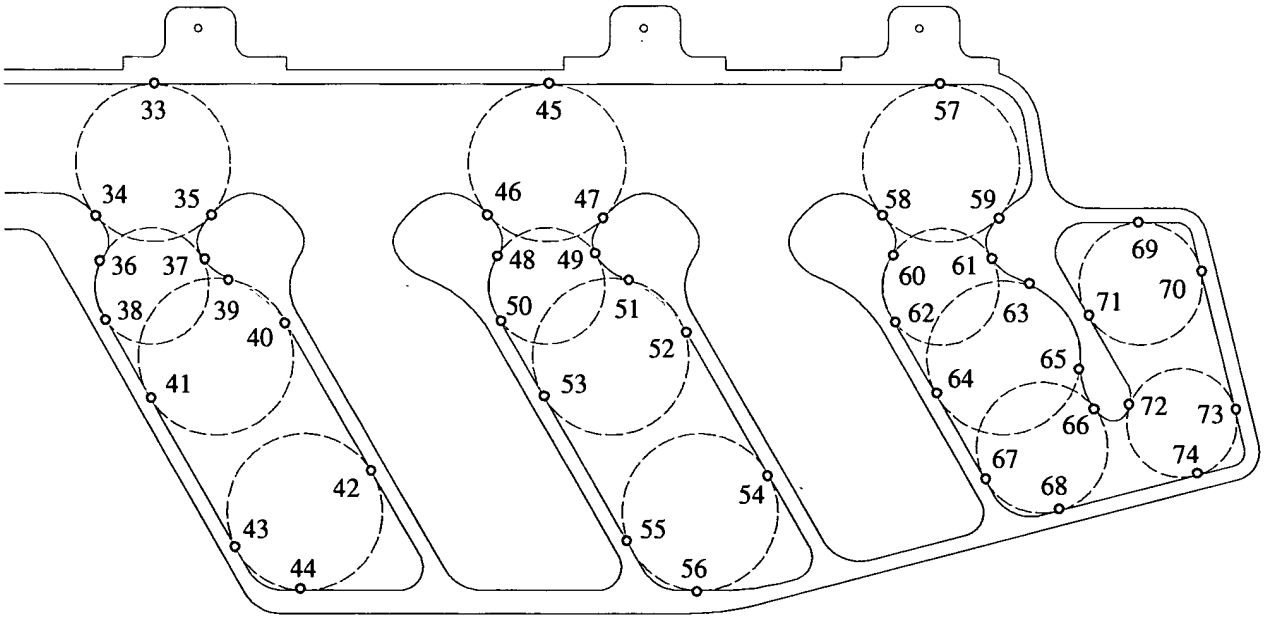

Fig. 14.2. Locations of points 33..74 where the peeling stress values have been determined in the adhesive joint that belongs to the right part of the airbag

14.3. Calculated results

The source data related to the points and calculated results are presented in the table below.

Point No.	d cm	r cm	k_l	ψ kg/cm
1	5.27	∞	1.00	1.68
2	5.27	4.80	1.20	3.78
3	5.27	8.98	1.40	3.45
4	5.23	∞	1.00	1.66
5	5.23	8.98	1.40	3.42
6	5.23	8.98	1.40	3.42
7	3.98	∞	1.00	1.27
8	3.98	0.80	1.00	6.31
9	3.98	0.80	1.00	6.31
10	3.70	4.80	1.20	2.28
11	3.70	2.71	1.40	3.45
12	3.70	∞	1.00	1.18
13	3.82	2.97	1.40	3.45
14	3.82	2.97	1.40	3.45
15	3.82	∞	1.00	1.22
16	3.95	4.80	1.20	2.50
17	3.95	∞	1.00	1.26
18	3.95	5.00	1.20	2.46
19	5.43	10.19	1.40	3.45
20	5.43	∞	1.00	1.73
21	5.43	∞	1.00	1.73
22	4.88	∞	1.00	1.55
23	4.88	∞	1.00	1.55
24	4.88	6.03	1.40	3.58
25	4.53	∞	1.00	1.44
26	4.53	4.68	1.40	3.58
27	4.53	∞	1.00	1.44
28	4.93	6.25	1.40	3.58
29	4.93	6.25	1.40	3.58
30	4.93	∞	1.00	1.57
31	5.43	15.20	1.40	3.11

Point No.	d cm	r cm	k_l	ψ kg/cm
32	5.43	-15.00	1.00	1.25
33	5.41	∞	1.00	1.72
34	5.41	8.91	1.40	3.58
35	5.41	8.91	1.40	3.58
36	3.99	3.15	1.40	3.58
37	3.99	3.15	1.40	3.58
38	3.99	∞	1.00	1.27
39	5.39	8.77	1.40	3.58
40	5.39	∞	1.00	1.72
41	5.39	∞	1.00	1.72
42	5.39	∞	1,00	1,72
43	5.39	∞	1.00	1.72
44	5.39	∞	1.00	1.72
45	5.41	∞	1.00	1.72
46	5.41	8.91	1.40	3.58
47	5.41	8.91	1.40	3.58
48	3.99	3.15	1.40	3.58
49	3.99	3.15	1.40	3.58
50	3.99	∞	1.00	1.27
51	5.39	8.77	1.40	3.58
52	5.39	∞	1.00	1.72
53	5.39	∞	1.00	1.72
54	5.39	∞	1.00	1.72
55	5.39	∞	1.00	1.72
56	5.39	∞	1.00	1.72
57	5.41	∞	1.00	1.72
58	5.41	8.91	1.40	3.58
59	5.41	8.91	1.40	3.58
60	3.99	3.15	1.40	3.58
61	3.99	3.15	1.40	3.58

Point No.	d cm	r cm	k_l	ψ kg/cm
62	3.99	∞	1.00	1.27
63	5.28	8.08	1.20	3.07
64	5.28	∞	1.00	1.68
65	5.28	8.08	1.20	3.07
66	4.50	4.58	1.40	3.58
67	4.50	∞	1.00	1.43
68	4.50	∞	1.00	1.43
69	4.19	∞	1.00	1.33
70	4.19	∞	1.00	1.33
71	4.19	∞	1.00	1.33
72	3.74	2.60	1.40	3.58
73	3.74	∞	1.00	1.19
74	3.74	∞	1.00	1.19

The obtained results should be treated as approximate and tentative. A more accurate finite-element analysis is recommended to refine the solution.

As the data of the table presented above show, the maximum peeling stress is found in the points 8 and 9 (see Fig. 13.1). This is caused by the rounding radius in the vicinity of those points which is too small. This radius should be increased to 3.5 cm near the points 8 and 9. In that case the peeling stress will never exceed the magnitude of 4 kg/cm under the internal pressure above ambient equal to 0.5 kg/cm^2 .

23. REFERENCES

[22]. Appendix 3. Experimental studies of a side impact inflatable head protector.

[23]. Appendix 4. Deformed shape and Stress state of side head protectors.

Appendix 6

RATIONAL SHAPES OF ADHESIVE JOINTS

Contents

24. COMMON CONSIDERATIONS

The glued or welded joint is a weakest place in a film airbag. So it is natural that one tries to minimize the ultimate peeling stress in seams of the bag. The easiest way to do it is to lower the pressure inside the airbag, decrease the sizes of the hollows etc. Though, these measures deprive the airbag of its efficiency. The author does not try to formulate any optimization problem here. Instead, the following approach is suggested.

As calculations show, the peeling stress is highly non-uniform along the joint's contour. In particular locations it rises to peaks several times higher than the average level. It is these peaks that determine the strength of the whole adhesive joint. The intensity of the peak stress depends very much on the shape of the joint's contour. Changing the contour's shape can eliminate the peaks and decrease the maximum peeling stress essentially. A perfect contour in this approach would be one with the same (uniform) stress in its every point.

So, the problem is how to find such shape of the adhesive joint wherein the stress along the contour is constant or nearly constant. This problem can be solved by making use of the approximate method described in paper [25].

25. BI-PERIODICAL MODEL OF AIRBAG

25.1. Derivation of equations

Let us consider the adhesive joint's contour of a hollow having a symmetry axis (Fig. 25.1). Let the branch of this contour located in the positive quarter be expressed by the functional relationship $y(x)$. As commonly known, the curvature of the branch can be described by the formula:

$$\kappa = \frac{y''}{(1+y'^2)^{3/2}}. \qquad (25.1)$$

Here and further the stroke denotes the differentiation with respect to x.

The sign of the curvature is positive when the convexity of the curve looks downwards.

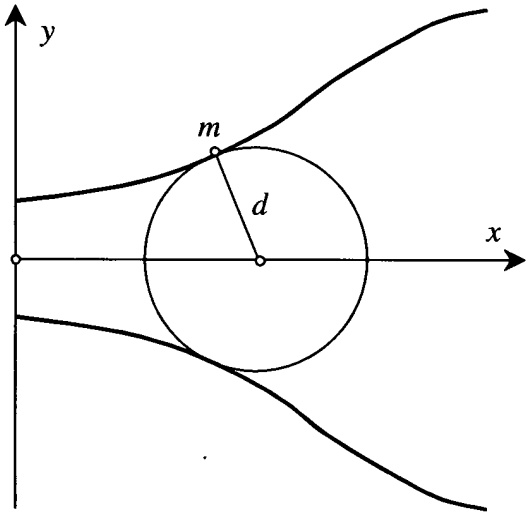

Fig. 25.1. The scheme of a hollow symmetrical with respect to the x axis

According to the procedure of the approximate method for determining the peeling stress, first a circle of the radius d should be inscribed in the hollow. As the hollow is symmetrical, its center will belong to the x axis. Let the point m where the circle and the curve touch each other have the coordinates x, y. Then

$$d = y\sqrt{1+y'^2}. \qquad (25.2)$$

As the bi-periodical configurations will, most probably, have convex adhesive joints, in order to find the peeling stress we will use the formula from [25], one that is true for convex fragments of the contour:

$$\psi = c_g c_l \frac{2pd}{\pi}(1+0.8\eta); \qquad (25.3)$$

$$\eta = \kappa d. \qquad (25.4)$$

The internal pressure p is not specified here because it has no effect on the result of the solution. The correction coefficients c_g, c_l will be assumed equal to one.

The differential equation to determine the contour's curve can be derived from the condition:

(25.5) $$\psi' = \frac{2p}{\pi}\left(d'(1+0.8\eta)+0.8d\eta'\right) = 0.$$

This condition has the following brief form:

(25.6) $$d'(1+0.8\eta)+0.8d\eta' = 0.$$

By substituting expressions from the formulae (25.1), (25.2) and (25.4) together with their derivatives in that expression, we obtain:

(25.7) $$y'\sqrt{1+y'^2} + \frac{yy'y''}{\sqrt{1+y'^2}} + 0.8\frac{\left(1+y'^2\right)\left(2yy'y'' + y^2y'''\right) - y^2y'y''^2}{\left(1+y'^2\right)^{3/2}} = 0.$$

Multiplying the equality (25.7) by the expression $\left(1+y'^2\right)^{3/2}$ will give us this equation:

(25.8) $$y'\left(1+y'^2\right)^2 + yy'y''\left(1+y'^2\right) + 0.8y\left[\left(1+y'^2\right)\left(2y'y'' + yy'''\right) - yy'y''^2\right] = 0.$$

This is a third-order differential equation to determine the functional relationship of $y(x)$. Introducing new variables y_1 and y_2 will turn the equation into a system of three ordinary first-order differential equations resolved with respect to derivatives:

(25.9) $$\begin{aligned} y' &= y_1; \\ y_1' &= y_2; \\ y_2' &= \frac{y_1}{4y^2}\left(\frac{4y^2y_2^2}{1+y_1^2} - 13yy_2 - 5(1+y_1^2)\right). \end{aligned}$$

Systems of this kind can be solved by the Runge–Kutta method.

25.2. Finding of rational glued area shape

Let us consider rational shapes of the joints in a square grid. The basic configuration is shown in Fig. 21.7.

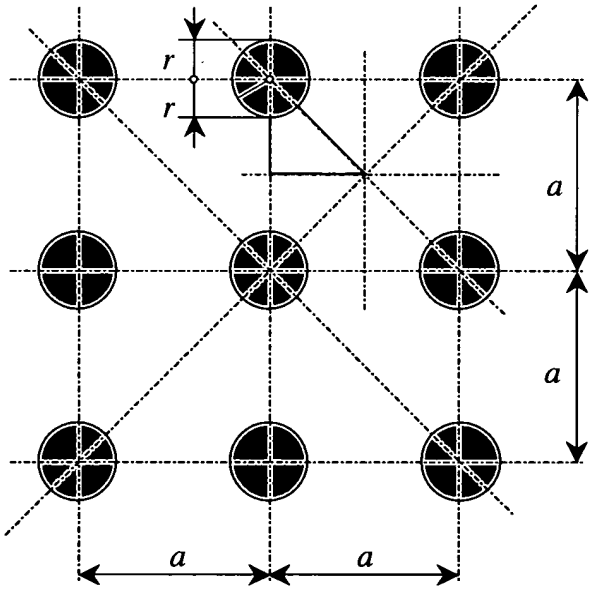

Fig. 25.2. A planar scheme of an airbag having a bi-periodical system of adhesive joints located in nodes of a square grid

In this figure the adhesive joints are shown schematically as circles. The rational shape of the joint will be different and more complex. As in the preceding case, the spacing of the grid is a and the radius of the joint along the coordinate axes is r.

Let's consider a part of the contour falling into an elementary cell marked by a color triangle in the figure (see Fig. 25.3). The curve is defined by the differential equation (25.8) or its equivalent system (25.9). Also, boundary conditions need to be specified. These follow:

$$
\begin{aligned}
& y = \frac{a}{2} - r \quad at \quad x = 0; \\
& y' = 0 \quad at \quad x = 0; \\
& y' = 1 \quad at \quad x + y = \frac{a}{2}.
\end{aligned}
\qquad (25.10)
$$

The first boundary condition sets up the required radius of the joint. The other two boundary conditions ensure a smooth transition of the curve to adjacent elementary cells.

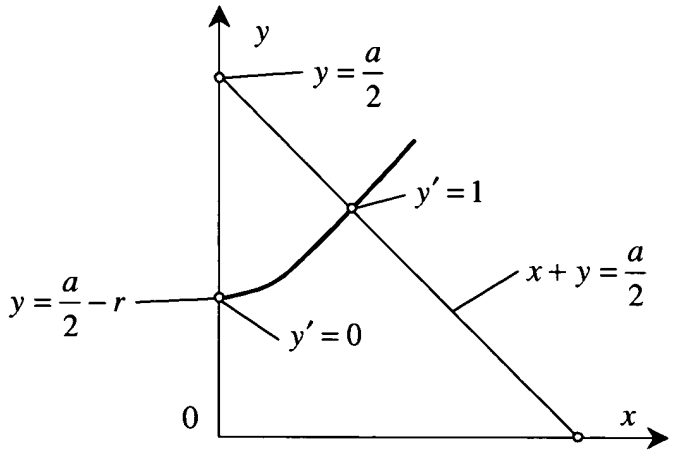

Fig. 25.3. Determining the shape of the joint's contour inside an elementary cell

The system of differential equations (25.9) has been integrated using the computer mathematics software Mathcad 2000 PRO at a = 10 cm for a sequence of five values of r: 1.0; 1.5; 2.0; 2.5; 3.0 cm. The curves obtained are shown in Fig. 25.4.

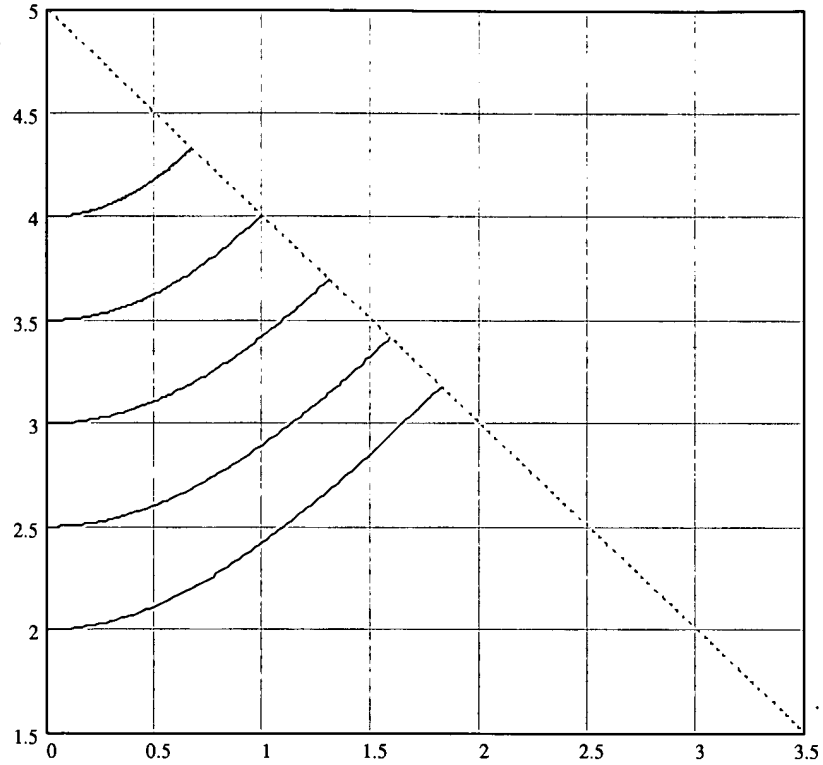

Fig. 25.4. Rational shapes of joints inside an elementary cell

The analysis of the airbag with these joints by the approximate method yields the uniform peeling stress along the whole contour. Values of the stress at the internal pressure above ambient $p = 1$ kg/cm^2 vs. the joint's radius are given in Table 15.

Table 15. The peeling stress ψ in kg/cm vs. the joint's radius r

r cm	1.0	1.5	2.0	2.5	3.0
ψ kg/cm	14.2806	8.7415	5.9503	4.2717	3.1596

25.3. Comparison with finite element method

Let's choose the curve that conforms to $r = 2$ cm for a more careful study. Numerical coordinates of points of the curve are presented in Table 16.

Table 16. Coordinates of the joint's contour points at $r = 2$ cm

x см	0.0000	0.1300	0.2600	0.3900	0.5200	0.6500	0.7800	0.9100	1.0400	1.1700	1.3000
y см	3.0000	3.0074	3.0297	3.0668	3.1182	3.1838	3.2630	3.3551	3.4593	3.5746	3.7000

The airbag with this joint's contour was analyzed by the finite element method. The analysis used these source data:

- thickness of the film sheet $h = 0.01$ cm;
- elasticity modulus $E = 36000$ kg/cm^2;
- Poisson ratio $\nu = 0.39$;
- grid spacing $a = 10$ cm;
- radius of the joint $r = 2$ cm;
- gas pressure above ambient $p = 1$ atmosphere.

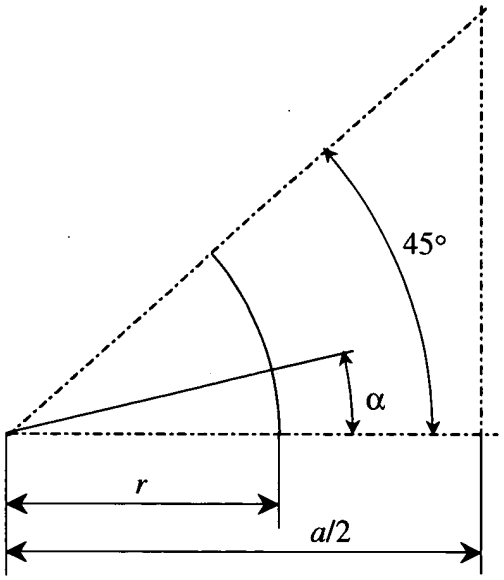

Fig. 25.5. A schematic of the elementary cell.

The shape and the sizes of the elementary cell are shown in Fig. 15.12. The division of the elementary cell into finite elements is shown on the deformed shape of the cell (Fig. 25.6). The peeling stress per unit of length thus obtained are shown as plots in Fig. 15.19. The same figure presents results of analysis of the same airbag with round adhesive joints reported in [24]. The ideal uniform peeling stress intensity is also shown in Fig. 15.19.

It should be noted that the joint's contour obtained by the suggested technique does not ensure a perfect distribution of the stress. Though, playing with the shape of the contour enables us to decrease the peeling stress by 20% or so.

The problem in question should be treated as a disadvantageous-class one because the stress concentration factor is not high here, and the approximate method provides a poor description of the peeling stress in the area of intensive fold formation at the angles $0 \leq \alpha \leq 20°$.

It is expected that for other types of problems the results should be of better quality.

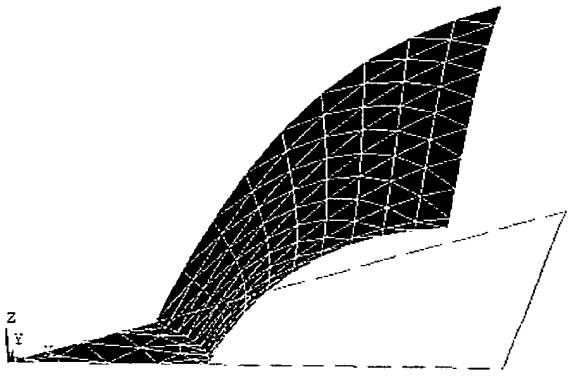

Fig. 25.6. The deformed shape of the elementary cell divided into finite elements

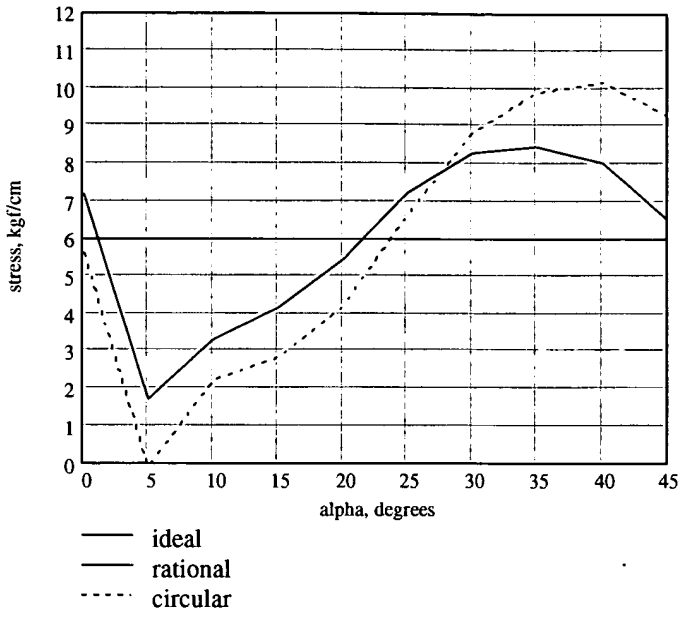

Fig. 25.7. The peeling stress per unit of length at the contour of the joint

It should be admitted that the technique of determining the rational shapes of the joints still needs improving.

26. BULB-LIKE CAPS AT RIGHT ANGLE JOINED HOLLOWS

This chapter deals with a problem of finding rational shapes of bulb-like caps that adhesive joints between two film sheets have. The subject of interest includes caps in locations where elongate hollows cross one another at the right angle (Fig. 26.1). The solution of the problem is based on an approximate method for determining the peeling stress [25].

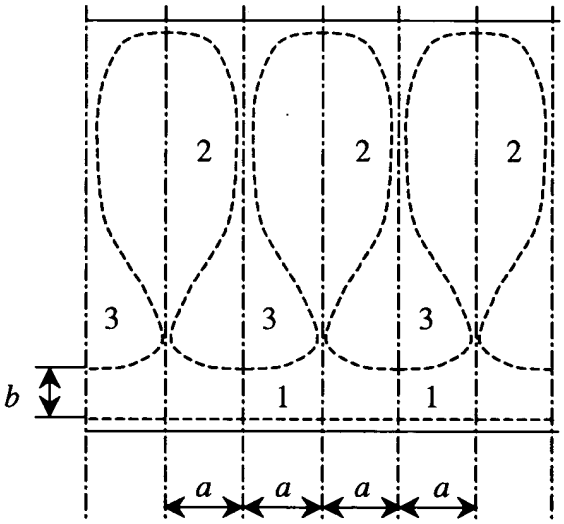

Fig. 26.1. A schematic of adhesive joints in locations of intersection of two elongate hollows (1) a hollow with a rectilinear edge; (2) a bisymmetric hollow; (3) an adhesive joint

26.1. Derivation of differential equations

The problem of a contour's rational shape includes finding such shape of the contour in which the stress along the contour is uniform. This problem has been addressed in the chapter 25 for the case

of an adhesive joint having a simple shape. The bulb-like caps have more complicated shapes which cannot be represented by single-valued functions in a Cartesian coordinate system. Therefore we are going to describe this shape in a parametrical way via the arc length s, in order to derive appropriate differential equations.

As Fig. 26.1 shows, the protector airbag is a periodical structure containing a hollow 1 with one rectilinear edge and a hollow 2 that possesses a bilateral symmetry (bisymmetry). Let's consider an elementary cell of this structure colored in Fig. 26.1 and use the inscribed circle method [25] on it.

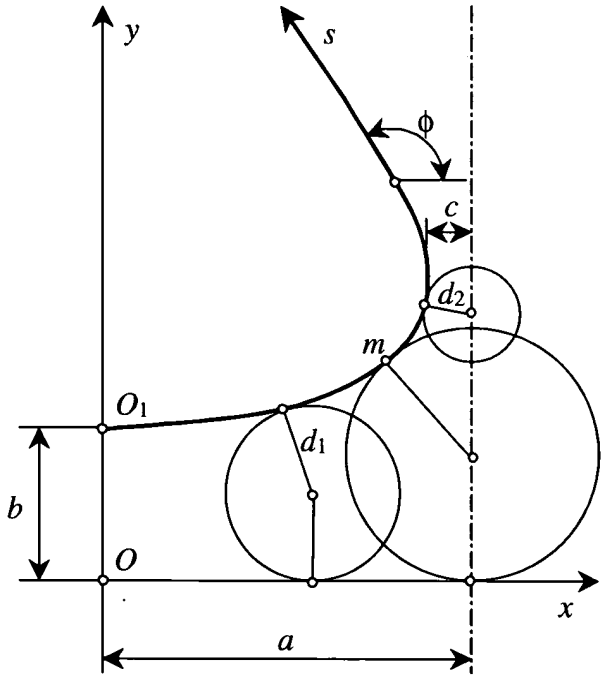

Fig. 26.2. To the determination of a rational shape of an adhesive joint

Let's refer the elementary cell to a Cartesian coordinate system xOy (Fig. 26.2) and consider the contour of the joint. We introduce an arc coordinate s, with its zero value conforming to the point O_1 and the coordinate itself increasing in the direction of the point m. Let the Cartesian coordinates of this contour be described by relationships $x(s)$, $y(s)$.

Let's now introduce the angle $\phi(s)$ between the positive direction of the x axis and that of the tangent to the curve (Fig. 26.2) as a function of the arc coordinate s. This function can be easily used to express the derivatives of the coordinates with respect to the arc length and the curvature of the contour:

(26.1) $\quad x' = \cos\phi;$

(26.2) $\quad y' = \sin\phi;$

(26.3) $\quad \kappa = \phi'.$

Here and further below the stroke denotes the differentiation with respect to s. The curvature's sign is positive if the convexity of the curve looks rightwards when moving along the curve towards the growth of the coordinate s.

Now take the hollow 1 and inscribe a circle of the radius d_1 in it. Geometrical considerations give us this:

$$d_1 = \frac{y}{1+\cos\phi}. \qquad (26.4)$$

For the hollow 2 the following formula will take place:

$$d_2 = \frac{a-x}{\sin\phi}. \qquad (26.5)$$

The formula (25.2) is true at a segment of the curve from the point O_1 to the point m whereat the center of the inscribed circle reaches the vertical line $x = a$, and the formula (26.5) works for the rest of the curve.

To derive the differential equations, we will use this formula for determining the peeling stress that holds at any point of the curve:

$$\psi = \frac{2pd}{\pi} f(\eta); \qquad (26.6)$$

where $\eta = \kappa d$;

ψ is the peeling stress;

p is the internal pressure above ambient;

d is the radius of the inscribed circle that touches the curve at the point of interest;

$f(\eta)$ is a function of a dimensionless parameter η defined in this way:

$$\begin{aligned} f(\eta) &= 1+\frac{4}{5}\eta && at \quad \eta \ge 0; \\ f(\eta) &= 1+\frac{4}{5}\eta\left(1-\frac{\eta^2}{3}\right) && at \quad -1 \le \eta < 0. \end{aligned} \qquad (26.7)$$

The formulae (26.6) and (26.7) are taken from the paper [25].

Notice that the domain of the function $f(\eta)$ is

$$-1 \le \eta < \infty, \qquad (26.8)$$

and its range of values is

$$\frac{7}{15} \le f < \infty. \qquad (26.9)$$

Values of $\eta < -1$ are not physical because no circle of a given radius can contain an inscribed circle of a greater radius.

The function $\eta(f)$ inverse to the function (26.7) is also of some interest. This is how it looks:

$$\begin{aligned} \eta(f) &= -2\cos\left[\frac{\pi+\alpha(f)}{3}\right] && at \quad \frac{7}{15} \le f < 1 \\ \eta(f) &= \frac{5}{4}(f-1) && at \quad 1 \le f < \infty \end{aligned} \quad ; \qquad (26.10)$$

where

$$\alpha(f) = \arccos\left[\frac{15}{8}(1-f)\right]. \qquad (26.11)$$

The function $\eta(f)$ in the formula (26.10) is an accurate inverse one to the function $f(\eta)$ specified by the formula (26.7).

It follows from the formula (26.6) that:

$$f(\kappa d)=\frac{\pi\psi}{2pd}; \qquad (26.12)$$

The inversion of the function f gives this:

$$\kappa d=\eta\left(\frac{\pi\psi}{2pd}\right). \qquad (26.13)$$

The principal differential equation follows from the formulae (26.13) and (25.1):

$$\phi'=\frac{1}{d}\eta\left(\frac{\pi\psi}{2pd}\right) \qquad (26.14)$$

This one and the equations (26.1), (26.2) together constitute a system of first-order differential equations resolved with respect to derivatives.

The value of d should be taken either from (25.2) if the point with the coordinates x, y is at the first segment, or from the formula (26.5) if the point with the coordinates x, y is at the second segment.

This fact can be established in the following way. If this inequality holds:

$$y\sin\phi<(a-x)(1+\cos\phi); \qquad (26.15)$$

then the point belongs to the segment 1, and if the inequality does not then the point is at the segment 2.

The initial conditions are known:

$$x(0)=0; \qquad (26.16)$$

$$y(0)=b; \qquad (26.17)$$

$$\phi(0)=0. \qquad (26.18)$$

The size b is shown in Fig. 26.2.

This system can be easily solved by the Runge–Kutta method.

26.2. Example solutions

Example 1. Consider a problem conforming to a schematic shown in Fig. 26.1 and Fig. 26.2 at a = 5.5 cm, b = 7.5 cm. It is required to determine a few feasible shapes of the joint's bulb-like cap.

The matter is that at the same initial conditions expressed by the formulae (26.16) - (26.18) we can build a whole family of rational joint's shapes by specifying different intensities of the peeling stress ψ. This will also change the width of the channel c (see Fig. 26.2). On the other hand, by specifying the channel's width we can obtain a particular value of the stress.

Let's adhere to the second formulation and build five curves that will conform to the channels of the widths c = 1 cm; 1.5 cm; 2 cm; 2.5 cm and 3 cm.

The problem has been solved using the computer mathematics software Mathcad 2000 PRO.

Shapes of the bulb-like caps in all five cases are shown in Fig. 26.3. This figure shows segments of the curves whereat uniform peeling stress levels have been achieved. Extensions of these curves can be designed according to practical considerations.

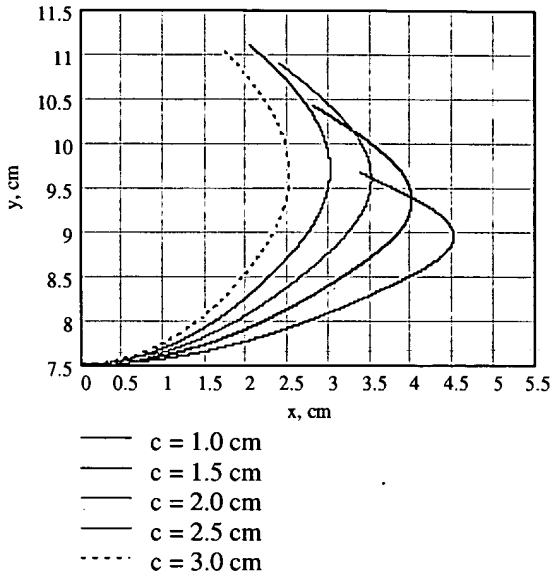

Fig. 26.3. Shapes of bulb-like caps

Each of the curves conform to a certain intensity of the peeling stress. These intensities are directly proportional to the internal pressure p above ambient inside the airbag. We can represent these stress intensities by the formula:

(26.19) $$\psi = U p;$$

and then values of U, with the dimension of length, will be a function of c.

This relationship is presented in the table below.

c, cm	1.0	1.5	2.0	2.5	3.0
U, cm	3.379	3.889	4.451	5.111	5.940

Example 2. Consider rowed bulb-like caps of a side curtain head protector airbag for the "Saturn" car. We take $a = 6.8$ cm; $b = 7.5$ cm; $c = 3.1$ cm (see Fig. 26.2).

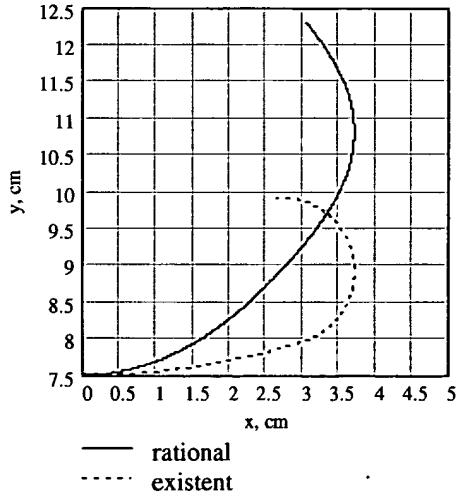

Fig. 26.4. A rational shape of the adhesive joint in a side curtain protector airbag for the "Saturn" car

A rational shape of the adhesive joint has been determined at these values of the parameters. It is shown in Fig. 26.4. The same figure also shows a dash curve that outlines the existing shape of the joint. Notice how much it is different from the calculated rational shape.

The peeling stress intensity at the rational contour of the joint obtained can be calculated by the formula (26.19), seeing that $U = 5.118$ cm.

Note that the mathematical relationships obtained in this report refer to the case when the axes of the lateral hollows 2 are perpendicular to the axis of the longitudinal hollow 1 (see Fig. 26.1). In the protector airbag for the "Saturn" car, the axes of the lateral hollows are oblique to the longitudinal axis. Therefore the rational shape of the joint obtained for this example is applicable only to a part of the bag nearest to the longitudinal hollow. The shape of the joint around the lateral hollow needs to be investigated further.

A finite-element analysis of the side curtain protector airbag for the "Saturn" car was carrying out at the internal pressure $p = 0.5$ kg/cm^2 above ambient. There, the peeling stress intensity in the area adjacent to the longitudinal hollow is as high as 8.9 kg/cm.

The stress at the boundary of the rational adhesive joint calculated by the formula (26.19) is a few times lower:

(26.20) $$\psi = 5.118 \cdot 0.5 = 2.559 \text{ kg/cm}.$$

Thus, the rational shape of the adhesive joint can give a substantial improvement of the design.

26.3. A validating finite-element analysis

Up to this point, the rational shape of the adhesive joint has been calculated using the approximate method of the peeling stress determination. So, it is quite natural that the shape of the joint is approximate too. The peeling stress is non-uniform along its contour, though it should not change along the contour in a perfect case.

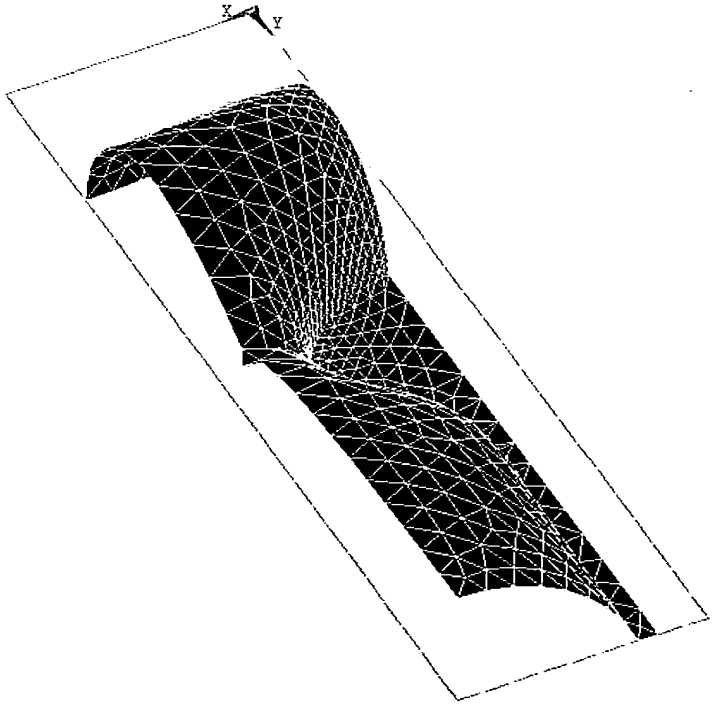

Fig. 26.5. Division of an elementary cell into finite elements and its deformed shape

So, a validating finite element analysis has been performed in order to estimate the proximity and efficiency of the previous approach. It used one of versions of the example 1 with the source data *a*

= 5.5 cm, b = 7.5 cm, c = 2.5 cm. The internal pressure above ambient was p = 0.5 kg/cm^2. The ANSYS software was used to perform the analysis.

Fig. 26.5 shows the division of the elementary cell into finite elements and its deformed shape when loaded. Then, Fig. 26.6 shows the numbering of points at the contour of the adhesive joint that helps one conveniently use the plot of the peeling stress presented in Fig. 26.7.

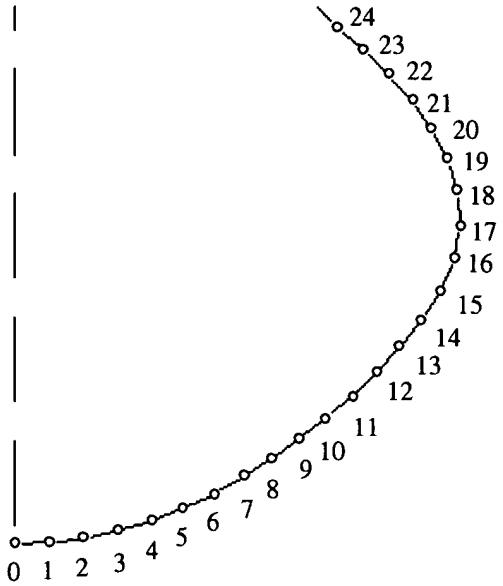

Fig. 26.6. Numbered points at the contour of the adhesive joint

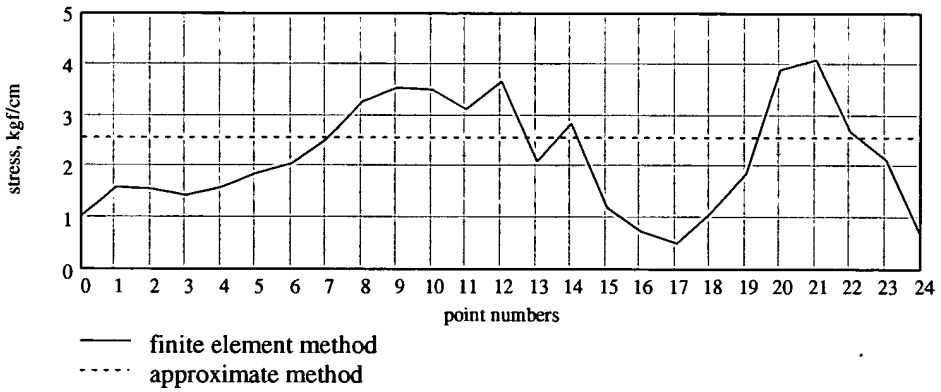

Fig. 26.7. Distribution of the stress along the adhesive joint's contour

This plot makes it clear that the peeling stress is distributed with a high non-uniformity along the contour of the adhesive joint. This is due to the fact that an intensive fold formation which can be observed in the vicinity of the points 15 through 19 is not taken into account explicitly by the approximate method. The simulated peeling stress flows away from this area to adjacent fragments of the contour thus making it higher 1.3–1.5 times in those parts. Nonetheless, even this high inaccuracy still lets us reduce the intensity of the stress two times or so by using the simulated rational shape.

27. BULB-LIKE CAPS AT OBLIQUELY JOINED HOLLOWS

The chapter 26 was dedicated to the determination of rational shapes of bulb-like end caps of adhesive joints between two film sheets. That chapter dealt with elongate hollows joined at the right

angles in mattress-like protection airbags. Though, there are numerous cases when these elongate hollows are joined at an angle other than right, that is, obliquely. It is exactly the problem of finding rational shapes of the adhesive joints with the hollows joined obliquely that this report deals with.

Two types of bulb-like caps for a "Saturn" car's side curtain airbag have been analyzed, and their rational shapes have been determined.

27.1. Geometry of an adhesive joint

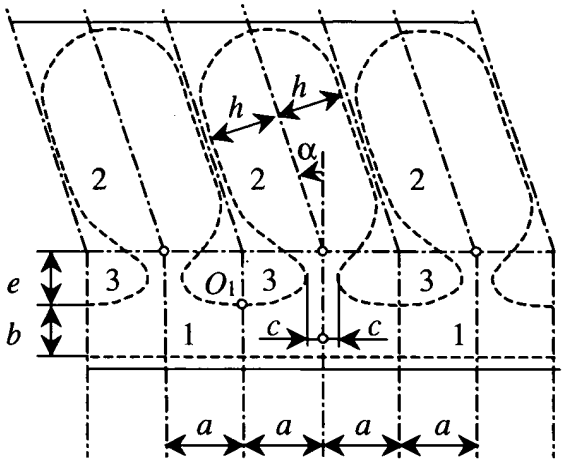

Fig. 27.1. A schematic of the joint.
(1) a hollow with a straight edge; (2) an oblique hollow; (3) an adhesive joint area

The object of consideration is a fragment of a side curtain airbag (Fig. 27.1) that has a longitudinal hollow 1 and a row of elongate hollows 2 at an oblique angle to the longitudinal one. The pressurized gas comes to the hollow 1 and then fills the hollows 2 passing through channels between the adhesive joints 3.

We assume that each of the channels has a symmetry axis perpendicular to the lower edge of the longitudinal hollow, and each of the elongate hollows has a symmetry axis at the angle α to the axis of its respective channel. These axes intersect at the axis inflection line.

The following sizes are marked in Fig. 27.1:

a is the half-spacing between the elongate hollows;

h is the half-width of the elongate hollow;

c is the half-width of the channel;

b is the width of the longitudinal hollow;

e is the distance from the top of the longitudinal hollow to the axis inflection line.

Knowing these sizes is enough to determine the rational shapes of the bulb-like caps of the adhesive joints in the case the hollows intersect obliquely.

27.2. Derivation of differential equations

The rational shape of the adhesive joint is such that the stress along the contour of the joint is constant. The problem is how to find the shape that meets this requirement.

As shown in Fig. 27.1, the object of interest is a periodical structure. Let's consider an elementary cell of this structure marked by color in this figure. The elementary cell contains a repeated fragment of the contour. It can be treated as consisting of two branches, right and left ones, separated by the O_1 point which is located at the vertical axis line of the adhesive joint (see Fig. 27.1). Let's consider the right branch first and derive differential equations for it by making use of the inscribed circle method [25].

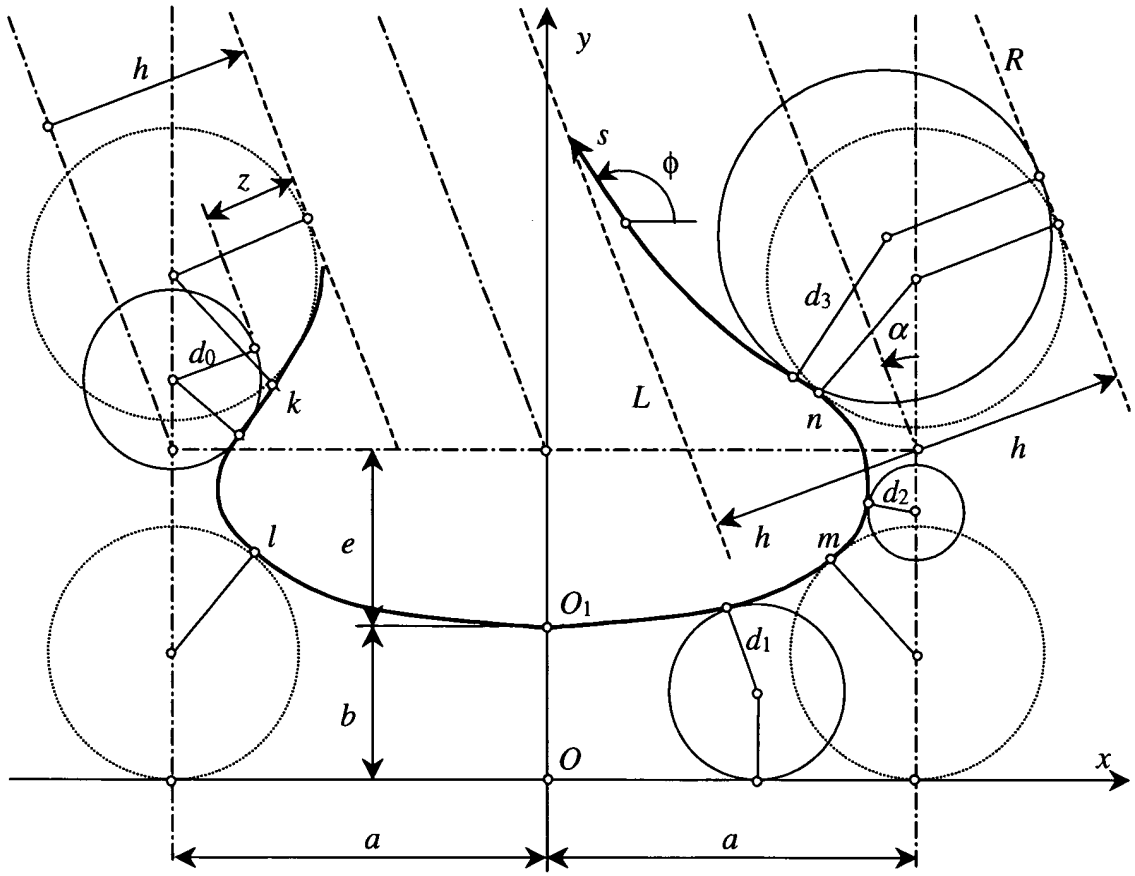

Fig. 27.2. To the determination of the rational shape of the adhesive joint

Let's refer the selected elementary cell to a Cartesian coordinate system xOy (Fig. 27.2) and deal with the contour of the joint. We introduce an arc coordinate s at the contour, with its zero value conforming to the O_1 point and its growing towards the m point. Let the Cartesian coordinates of the contour be expressed by relationships $x(s)$, $y(s)$.

Let us introduce an angle $\phi(s)$ into consideration — one between the positive direction of the x axis and the positive direction of the tangent to the curve (Fig. 27.2) — as a function of the arc coordinate s. This function can be used to express derivatives of the coordinates with respect to the arc length, and the curvature of the joint's contour:

(27.1) $x' = \cos\phi;$

(27.2) $y' = \sin\phi;$

(27.3) $\kappa = \phi'.$

Here and further the stroke denotes the differentiation with respect to s. The curvature sign is positive if the convexity of the curve looks rightwards when moving along the curve towards the growth of the s coordinate.

Let's consider the hollow 1 and inscribe a circle of a radius d_1 in it. Geometrical considerations give

(27.4) $$d_1 = \frac{y}{1+\cos\phi}.$$

This relationship is true for the fragment of the curve from the point O_1 to the point m where the center of the inscribed circle reaches the vertical line $x = a$. The channel area begins immediately farther.

The following formula for the inscribed circle's radius is true for the channel area between the points m and n:

$$(27.5) \qquad d_2 = \frac{a-x}{\sin\phi}.$$

The center of the inscribed circle should move along the vertical line $x = a$ until it touches one of the oblique lines L or R. The size e should be chosen so that the channel area be located between the oblique lines L and R.

If the inscribed circle has touched the L line first, then the process of constructing the right branch is over. If it has touched the R line first, then the branch should be continued. The tangent point of the inscribed circle will move along the R line. The radius of this circle can be determined by the formula:

$$(27.6) \qquad d_3 = \frac{(a-x)\cos\alpha + (b+e-y)\sin\alpha + h}{1+\sin(\phi-\alpha)}.$$

The process of the branch construction will complete when the radius of the circle d_3 reaches the value of h.

The left branch consists of at least two segments. The first of those begins at the k point. At this point the inscribed circle touches the right edge of the oblique hollow. This segment bounds the channel area and ends at the l point. The radius of the inscribed circle in an arbitrary point of this segment is:

$$(27.7) \qquad d_0 = -\frac{a+x}{\sin\phi}.$$

The gap between this circle and the right edge of the oblique hollow z can be calculated by the formula:

$$(27.8) \qquad z = -(x+a)\cos\alpha + (b+e-y)\sin\alpha + h + \frac{a+x}{\sin\phi}(1+\sin(\phi-\alpha)).$$

At $z = 0$ the inscribed circle touches the right edge of the oblique hollow.

Then goes the second segment. It begins at the point l and ends at the point O_1. This segment conforms to the first segment of the right branch by the principles of its construction. The radius of the inscribed circle at this segment can be calculated by the formula (25.2).

To derive the differential equations, we will use the following formula for the determination of the peeling stress which is true for any point of the curve:

$$(27.9) \qquad \psi = \frac{2pd}{\pi} f(\eta);$$

where $\eta = \kappa d$;

ψ is the peeling stress;

p is the internal pressure above ambient;

d is the radius of the inscribed circle that touches the curve at the point of interest;

$f(\eta)$ is a function of a dimensionless parameter η defined as follows:

$$
\begin{aligned}
& f(\eta)=1+\frac{4}{5}\eta && at\ \ \eta\geq 0; \\
& f(\eta)=1+\frac{4}{5}\eta\left(1-\frac{\eta^2}{3}\right) && at\ \ -1\leq\eta<0.
\end{aligned}
\qquad (27.10)
$$

The formulae (26.6) and (26.7) are borrowed from the paper [25].

Note that the domain of the function $f(\eta)$ is

$$-1\leq\eta<\infty, \qquad (27.11)$$

while its range of values is

$$\frac{7}{15}\leq f<\infty. \qquad (27.12)$$

Values of $\eta<-1$ are not physical because no circle of a given radius can contain an inscribed circle of a bigger radius.

The function $\eta(f)$ inverse to the function (26.7) is also of some interest.

This function is:

$$
\begin{aligned}
& \eta(f)=-2\cos\left[\frac{\pi+\alpha(f)}{3}\right] && at\ \ \frac{7}{15}\leq f<1 \\
& \eta(f)=\frac{5}{4}(f-1) && at\ \ 1\leq f<\infty
\end{aligned}
\quad ; \qquad (27.13)
$$

where

$$\alpha(f)=\arccos\left[\frac{15}{8}(1-f)\right]. \qquad (27.14)$$

The function $\eta(f)$ in the formula (26.10) is an accurate inversion of the function $f(\eta)$ specified by the formula (26.7).

It follows from (26.6) that:

$$f(\kappa d)=\frac{\pi\psi}{2pd}; \qquad (27.15)$$

or, after inverting the function f:

$$\kappa d=\eta\left(\frac{\pi\psi}{2pd}\right). \qquad (27.16)$$

The formula (26.13) gives the principal differential equation after taking (25.1) into account:

$$\phi'=\frac{1}{d}\eta\left(\frac{\pi\psi}{2pd}\right). \qquad (27.17)$$

This one together with the equations (26.1) and (26.2) make a system of three first-order differential equations resolved with respect to the derivatives.

The value of d should be calculated by the formula (25.2) if the point with the coordinates x, y is located at the first segment (before the m point), by the formula (26.5) if the point with the coordinates x, y is at the second segment (between the m and n points), or by the formula (27.6) if the point with the x, y coordinates is at the third segment (after the n point).

This statement can be proved as follows. If the following inequality holds:

(27.18) $$y\sin\phi < (a-x)(1+\cos\phi);$$

then the point belongs to the segment 1, otherwise to the segment 2.

The initial conditions are known:

(27.19) $$x(0) = 0;$$

(27.20) $$y(0) = b;$$

(27.21) $$\phi(0) = 0.$$

The b size is shown in Fig. 27.2.

The system can be solved easily by the Runge – Kutta method.

27.3. The shape of the bulb-like cap

We suggest the following principle for building the curvilinear contour of the bulb-like cap (Fig. 27.3).

First, the calculated part of the contour connecting the points k, l, m, n, o is built in the way described in Section 27.2. Note that the lower part of the contour is symmetric with respect to the y axis. In particular, the following relationships hold for the coordinates of the points:

(27.22) $$x_k = -x_n; \qquad y_k = y_n;$$

(27.23) $$x_l = -x_m; \qquad y_l = y_m.$$

Here and further we use the coordinate system presented in Fig. 27.2. Literal subscripts of the variables refer to characteristic points.

The contour segment j to k is a circular arc that joins smoothly the curvilinear contour and the rectilinear edge of the elongate hollow. The radius of this circle can be calculated by the formula

(27.24) $$r_1 = -\frac{a + x_k}{\sin\phi_k};$$

where x_k and ϕ_k are the coordinate x and angle ϕ at the point k, respectively.

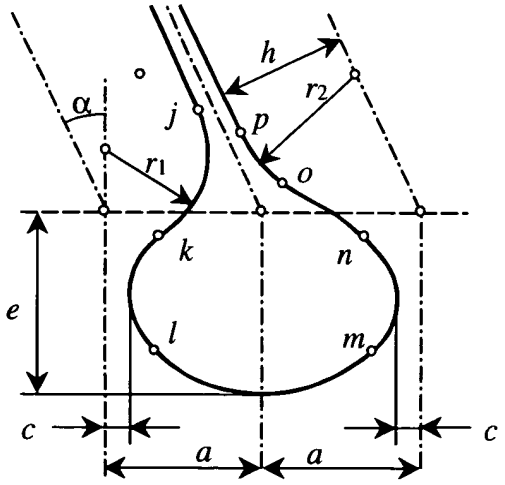

Fig. 27.3. The outline of the bulb-like cap

The coordinates of the circle's center can be found by the formulae:

(27.25) $$x_1 = -a;$$

(27.26) $$y_1 = y_k + r_1 \cos\phi_k .$$

The coordinates of the point j whereat the circle arc ends, are expressed by the formulae:

(27.27) $$x_j = -a - r_1 \cos\alpha ;$$

(27.28) $$y_j = y_k + r_1(\sin\alpha - \cos\phi_k).$$

The contour's segment o to p is a circular arc that connects the curvilinear contour with the rectilinear edge of the elongate hollow at the point o smoothly. The radius of the circle is h, and the coordinates of the center can be calculated by these formulae:

(27.29) $$x_2 = x_o + h\sin\phi_o ;$$

(27.30) $$y_2 = y_o - h\cos\phi_o .$$

The coordinates of the point p can be calculated by the formulae:

(27.31) $$x_p = x_o + h(\sin\phi_o - \cos\alpha);$$

(27.32) $$y_p = y_o - h(\cos\phi_o + \sin\alpha).$$

27.4. Bulb-like caps for a "Saturn" car's side curtain airbag

The side curtain airbag for the "Saturn" car consists of hollows of two types inclined at an oblique angle to the longitudinal axis of the airbag and to the longitudinal gas-distributing hollow (see Fig. 27.4). The first type is in the left part of the airbag, and the second type is in its right part. These two types are different in their inclination angles and some of their sizes. Let's consider each type separately.

The first type has the following dimensions:

a = 6.5 cm; b = 7.5 cm; c = 2.8 cm; e = 2.23 cm; h = 5.4 cm; α = 0.421.

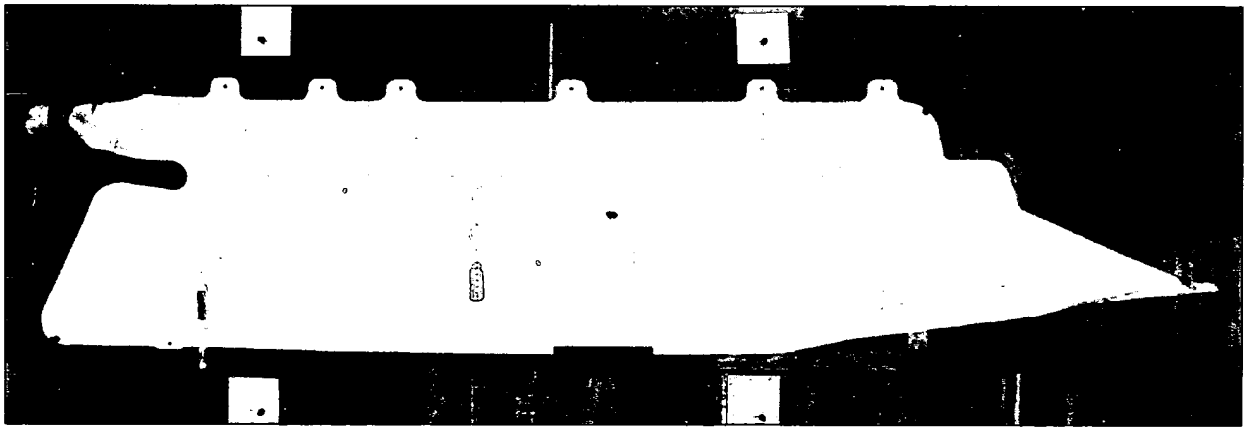

Fig. 27.4. A side curtain airbag for the "Saturn" car

The problem for this hollow type has been solved by the technique described above using the computer mathematics software Mathcad 2000 PRO. The results are presented graphically in Fig. 27.5 in coordinates conforming to Fig. 27.2. As can be clearly seen in this figure, the rational shape of the cap is essentially different from the one used in practice.

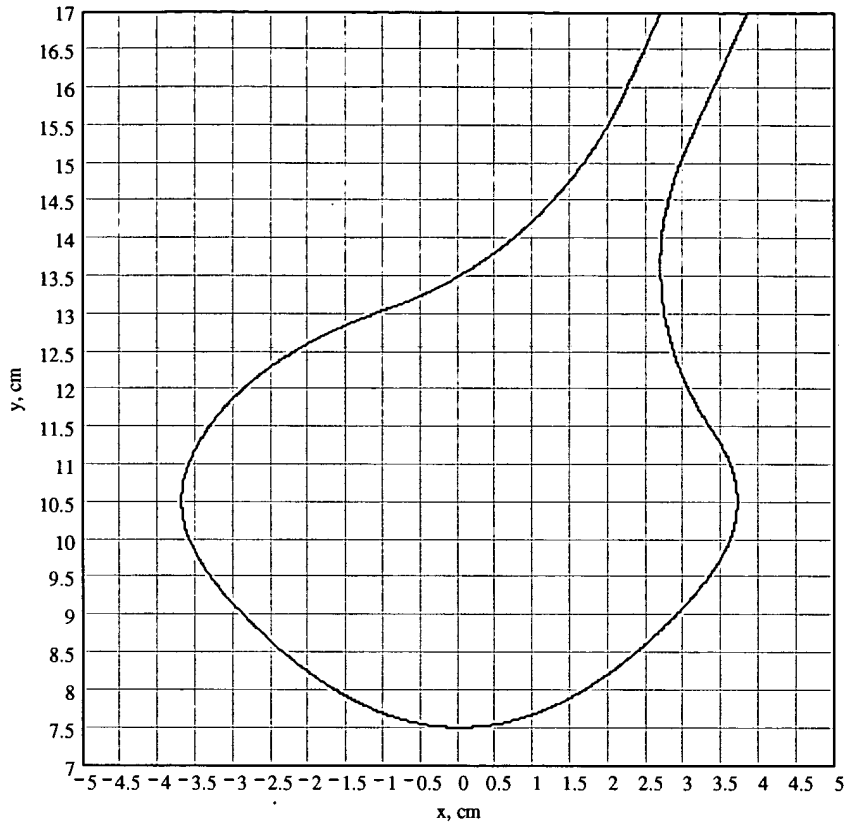

Fig. 27.5. The outline of the bulb-like cap for the first hollow type in its natural size

The level of the peeling stress at the contour of the cap can be calculated by the following formula, according to the approximate analysis technique:

(27.33) $\psi = U p;$

where p is the internal pressure above ambient inside the airbag;

U is a coefficient that depends on the shape of the cap.

In this case $U = 4.93$ cm.

The second type of the hollow has the following dimensions:

$a = 6.8$ cm; $b = 7.5$ cm; $c = 3.1$ cm; $e = 2.6$ cm; $h = 5.4$ cm; $\alpha = 0.52364$.

Necessary calculations have been performed for the cap with these properties, too. The determined shape of the cap is shown in Fig. 27.6.

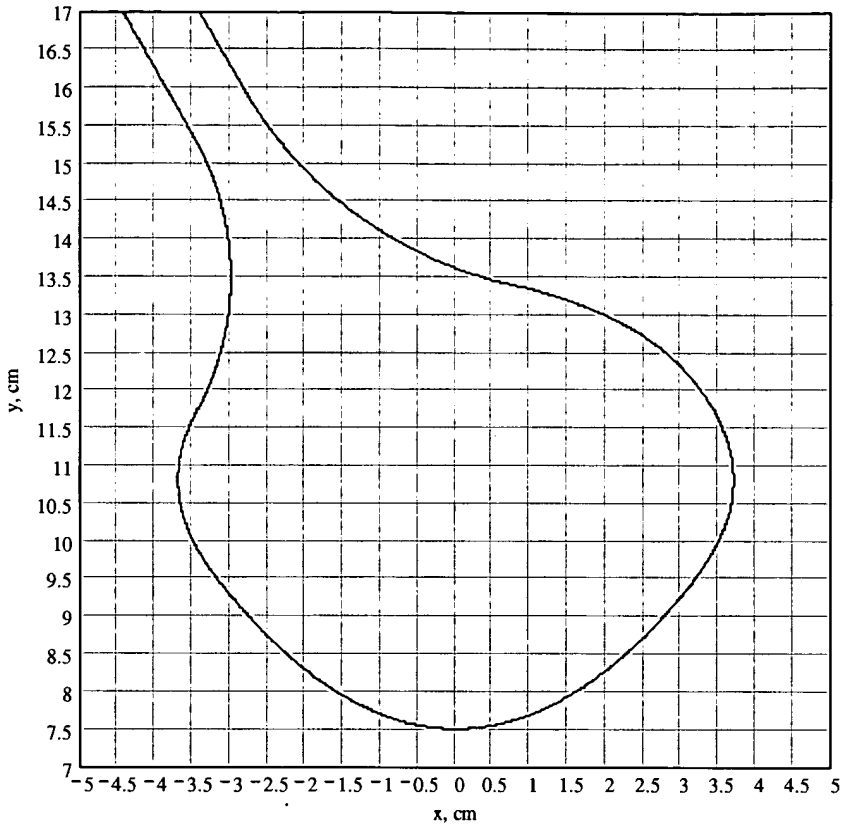

Fig. 27.6. The outline of the bulb-like cap for the second hollow type in its natural size

The level of the peeling stress for this cap can be calculated by the formula (26.19), assuming U = 5.118 cm.

A finite-element analysis of the side curtain airbag for the "Saturn" car was carried up at the internal pressure p = 0.5 kg/cm^2 above ambient. In that case the peeling stress in the area adjacent to the longitudinal hollow is as high as 8.9 kg/cm.

The stress at the boundary of the adhesive joint calculated by the formula (26.19) are as follows for the first hollow type:

(27.34) $\psi = 4.93 \cdot 0.5 = 2.465$ kg/cm;

for the second hollow type:

(27.35) $\psi = 5.118 \cdot 0.5 = 2.559$ kg/cm.

In either case the stress intensity is much lower than that in the real airbag. Even if we assume that the actual stress in the airbag is going to be 1.5 times higher than that calculated by the formulae (27.34) and (27.35), all the same the effect of the rational cap's shape will be noticeable.

28. LARGE HOLLOWS DIVIDED INTO PARTS

In some cases one needs to find how to reduce the peeling stress at the boundary of a large-scale hollow. With this purpose, one can arrange adhesive joints as separate small islands which turn a single-connected hollow into a double-connected one (Fig. 28.1), or as peninsulas which divide the large hollow into two smaller connected hollows (Fig. 28.2).

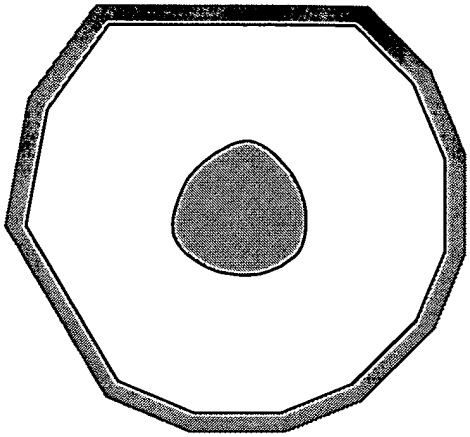

Fig. 28.1. A hollow with an isolated island-type adhesive joint.

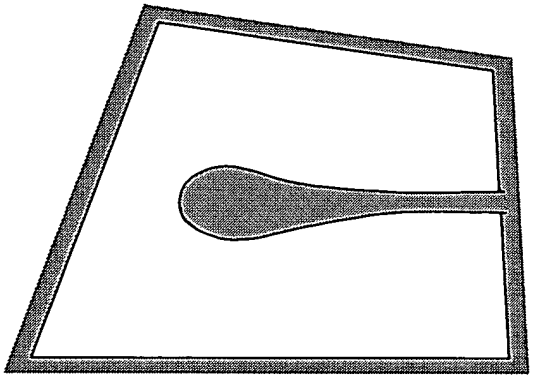

Fig. 28.2. A hollow with an isolated peninsula-type adhesive joint..

This chapter presents an attempt to solve the problem in the case when the large hollow is of a convex shape and its boundary consists of a finite number of linear segments.

28.1. Derivation of differential equations

As was done in chapters 25 and 26, here we seek such shape of the adhesive joint that the peeling stress is uniform along the boundary of the joint. Let's derive differential equations by following the inscribed circle method presented in [25].

We refer the area of interest to a Cartesian coordinate system, xOy (Fig. 28.3). Then, an arc length coordinate s is introduced at the boundary. The direction of its growth will be such that the hollow is on the right when moving along the curve in this direction. Let the Cartesian coordinates of the contour be defined by relationships $x(s)$, $y(s)$.

Now consider the angle $\phi(s)$ between the positive direction of the x axis and the positive direction of the tangent to the curve (Fig. 28.3) as a function of the arc coordinate s. This function can be used to easily express the derivatives of the coordinates with respect to the arc length, and the curvature of the joint's contour:

(28.1) $\quad x' = \cos\phi;$

(28.2) $\quad y' = \sin\phi;$

(28.3) $\quad \kappa = \phi'.$

Here and further, the stroke denotes the differentiation with respect to s. The sign of the curvature is positive if the convexity of the curve points rightwards as we move along the curve towards bigger s.

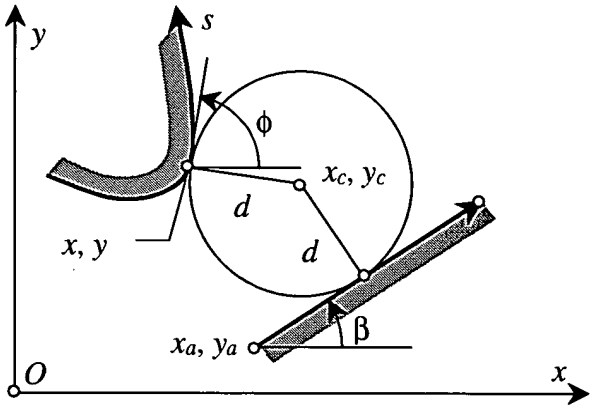

Fig. 28.3. Parameters of the adhesive joint's geometry

First, let's consider one rectilinear segment of the boundary specified by the coordinates of a point a belonging to it and by the angle β between the positive direction of the x axis and the positive direction of the boundary segment. The positive direction of the contour is such that the hollow is on the left.

The distance from the point with the coordinates x_c, y_c to this segment can be expressed by the formula:

$$d = -(x_c - x_a)\sin\beta + (y_c - y_a)\cos\beta. \qquad (28.4)$$

The coordinates of the center of a circle having the radius d and touching the contour of interest at the point with the coordinates x, y are defined by these formulae:

$$x_c = x + d\sin\phi; \qquad (28.5)$$

$$y_c = y - d\cos\phi. \qquad (28.6)$$

Substituting the expressions (28.5) and (28.6) to (28.4) will give us the following equation for determining the inscribed circle's radius d.

$$d = -(x + d\sin\phi - x_a)\sin\beta + (y - d\cos\phi - y_a)\cos\beta. \qquad (28.7)$$

This equation yields the following:

$$d = \frac{-(x - x_a)\sin\beta + (y - y_a)\cos\beta}{1 + \cos(\phi - \beta)}. \qquad (28.8)$$

To derive the desirable differential equations, we will use the following formula of the peeling stress that is true at any point of the contour:

$$\psi = \frac{2pd}{\pi} f(\eta); \qquad (28.9)$$

where $\eta = \kappa d$;

ψ is the peeling stress;

p is the internal pressure above ambient;

d is the radius of an inscribed circle touching the contour at the point of interest;

$f(\eta)$ is a function of a dimensionless parameter η defined as follows:

$$
\begin{aligned}
& f(\eta)=1+\frac{4}{5}\eta && at \quad \eta \geq 0; \\
& f(\eta)=1+\frac{4}{5}\eta\left(1-\frac{\eta^2}{3}\right) && at \quad -1 \leq \eta < 0.
\end{aligned}
\qquad (28.10)
$$

The formulae (26.6) and (26.7) are taken from the paper [25].

Next, consider the function $\eta(f)$ inverse to the function (26.7). It has the following form:

$$
\begin{aligned}
& \eta(f)=-2\cos\left[\frac{\pi+\alpha(f)}{3}\right] && at \quad \frac{7}{15} \leq f < 1 \\
& \eta(f)=\frac{5}{4}(f-1) && at \quad 1 \leq f < \infty
\end{aligned}
\qquad (28.11)
$$

;

where

$$
\alpha(f)=\arccos\left[\frac{15}{8}(1-f)\right]. \qquad (28.12)
$$

The function $\eta(f)$ in the formula (26.10) is an exact inversion of the function $f(\eta)$.
It follows from the formula (26.6) that:

$$
f(\kappa d)=\frac{\pi\psi}{2pd}; \qquad (28.13)
$$

and the inversion of the function f will give:

$$
\kappa d=\eta\left(\frac{\pi\psi}{2pd}\right). \qquad (28.14)
$$

The main differential equation follows from the formula (26.13) with (25.1) taken into account:

$$
\phi'=\frac{1}{d}\eta\left(\frac{\pi\psi}{2pd}\right). \qquad (28.15)
$$

This one together with the equations (26.1) and (26.2) make up a system of three first-order differential equations resolved with respect to derivatives.

28.2. Determination of a segment where an inscribed circle touches

The formula (28.8) can be used to calculate the radius of the tangent circle. One of its tangent points belongs to a line that bounds the area in question. There are several bounding lines of this kind. For each of those, an inscribed circle can be constructed and its radius determined. Obviously, only a circle of the least radius will be a truly inscribed one. This will be the one to indicate the segment that touches the inscribed circle.

Let's analyze the formula (28.8). The numerator of this formula is the distance between the point with the coordinates x, y to the segment in question. This can be made sure by considering the formula (28.4). The distance is signed — its sign is positive if the point is inside the area or negative if the point is outside. The adhesive joint is inside the area, therefore the numerator of the formula is positive. The denominator of the formula (28.8) is nonnegative. It can be equal to zero when the direction of the tangent to the curve is opposite to that of the area's boundary segment (Fig. 28.4).

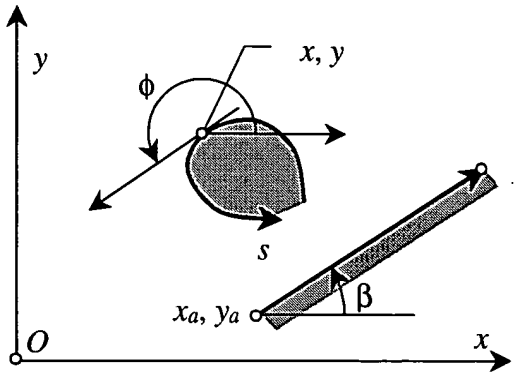

Fig. 28.4. A case when the denominator in (28.8) is equal to zero

In this case the radius of the circle calculated by the formula (28.8) becomes infinite. To avoid this inconvenience, we can modify the formulae by using a quantity opposite to the radius d of the circle, the curvature of the circle. Then the differential equation (28.15) will become this:

$$\phi' = q\eta\left(\frac{q\pi\psi}{2p}\right); \qquad (28.16)$$

The curvature of the circle can be calculated by the following formula:

$$q = \frac{1+\cos(\phi-\beta)}{-(x-x_a)\sin\beta+(y-y_a)\cos\beta}; \qquad (28.17)$$

with no risk that the denominator may become zero.

The inscribed circle will touch the segment at which the curvature q is maximum.

28.3. Principles for constructing the adhesive joints

Isolated island-type adhesive joints will be obtained by calculation, so their construction does not require any artificial technique. The complexity of the job is how to choose the initial values $x(0)$, $y(0)$, $\phi(0)$ so that a smooth closed curve could be obtained. The peeling stress ψ at the contour which arises under the internal pressure p above ambient, can be specified arbitrarily at one's will. As follows from the formula (28.16), it suffices to specify the ratio between the two values:

$$U = \frac{\psi}{p}. \qquad (28.18)$$

One of ways for choosing the initial values can be the following (Fig. 28.5). In the central part of the area we choose a line parallel to the x axis. Its equation is:

$$y = y(0). \qquad (28.19)$$

The initial point of the curve in question will be placed on this curve, which defines one of the initial conditions $y(0)$. The other two conditions are determined by an exhaustive search. For this purpose, the initial point is moved along the selected line to vary the initial condition $x(0)$. At last, the inclination angle of the curve at the initial point $\phi(0)$ can be varied. The purpose of this is to make the coordinate x and the angle ϕ same as they are at the initial point.

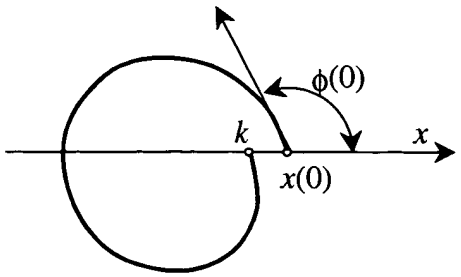

Fig. 28.5. Constructing the contour of the adhesive joint

An adhesive joint of the peninsula type (Fig. 28.6) consists of a neck (*a*, *b*, *f*, *g*), an end cap (*c*, *d*, *e*), and matching segments (*b*, *c*, *e*, *f*). The specified level of the stress (supposedly, uniform along the contour) can be found at the end cap's contour only. At the rest of the joint's contour, the stress is generally lower.

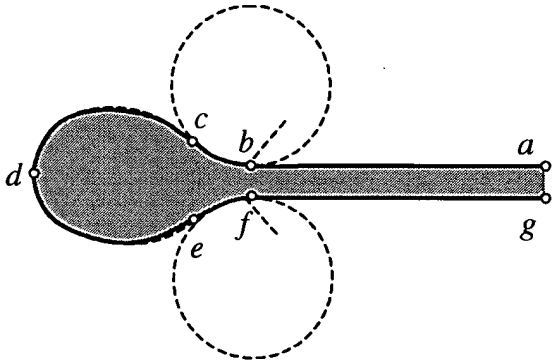

Fig. 28.6. Constructing a peninsula-type joint

The end cap's contour will be designed at an engineer's decision, and the shape of the contour will be found by solving a system of differential equations with initial conditions chosen approximately. The neck's properties will be determined from engineering considerations. The matching segments will follow a circular arc that joins smoothly to both the end cap and the neck. The radius (curvature) of this circular arc is of no real importance.

28.4. Example solutions

Problem 1. Find the shape of the bulb-like end cap in the left part of the "Saturn" car airbag head protector.

The big hollow in the left part of the "Saturn" car's side airbag head protector is bounded by three straight lines. The arrangement of those is shown in Fig. 27.4. Table 17 presents coordinates x_a, y_a of points belonging to each segment of the boundary and the angle β between the positive direction of the x axis and that of the boundary segment; the angle is provided in radians.

Table 17. Numerical data regarding the boundaries of the left hollow

No.	x_a (cm)	y_a (cm)	β
1	389.1007	436.7440	3.02225
2	291.7337	441.2023	-1.97747
3	234.6384	244.6773	0

Inside this area, a lot of curves can be built to provide for the uniformity of the peeling stress. The following data can be specified at the analyst's will: the intensity of the stress, the coordinates of one of the curve's points (at $s = 0$), and the direction of the curve at this point.

The stress intensity is described by the quantity U which is nothing but the ratio of the peeling stress vs. the pressure above ambient inside the airbag.

In the present example, this quantity is assumed to be the same as those in other joints of the airbag, and the initial conditions are assumed by engineering considerations:

(28.20) $U = \psi/p = 51.18$ mm;

(28.21) $x(0) = 322.7183$ mm;

(28.22) $y(0) = 345.4102$ mm;

(28.23) $\phi(0) = -2.98771$.

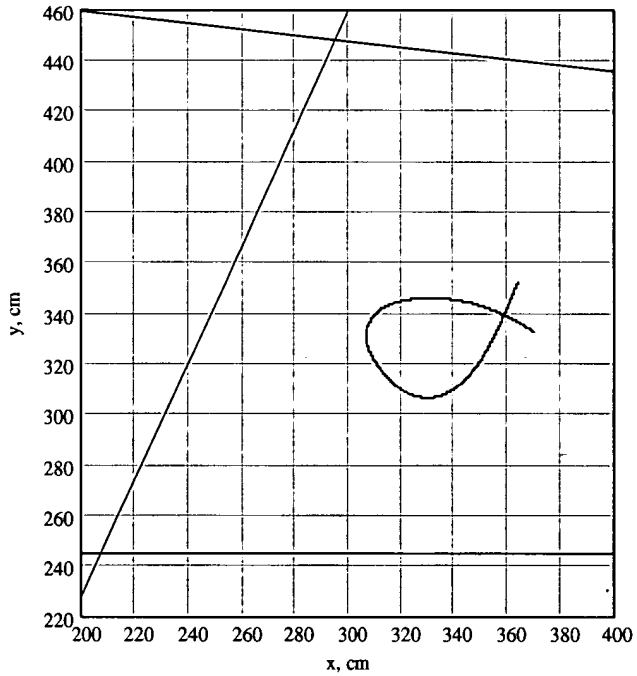

Fig. 28.7. The outline of the end cap in the left hollow

The curve obtained according to these conditions is shown in Fig. 28.7. This curve crosses itself. It can be used as a contour for the bulb-like end cap in an additional peninsula-type adhesive joint as shown in Fig. 28.2.

It is this curve that was used to determine the shape of the bulb-like cap in the left part of the "Saturn" car's side airbag head protector.

Problem 2. Determine the shape of the bulb-like end cap in the right part of the "Saturn" car's side airbag head protector.

The big hollow in the right part of the "Saturn" car's side airbag head protector is bounded by four straight lines. The arrangement of those is shown in the drawing of the airbag presented in Fig. 27.4. Table 18 presents coordinates x_a, y_a of points belonging to each segment of the boundary and the angle β between the positive direction of the x axis and that of the boundary segment; the angle is provided in radians.

Table 18. Numerical data regarding the boundaries of the right hollow

No.	x_a (cm)	y_a (cm)	β
1	1571.29	296.86	-1.0472
2	1571.29	296.86	0.25541
3	1693.29	503.86	1.81248
4	1693.29	503.86	3.14159

In this example, the stress intensity is assumed to be the same as that in other adhesive joints of the airbag. The initial conditions are assumed on the basis of engineering considerations, exactly as they were in the previous example:

(28.24) $U = \psi/p = 51.18$ mm;

(28.25) $x(0) = 1651.43$ mm;

(28.26) $y(0) = 393.6$ mm;

(28.27) $\phi(0) = 2.0944$.

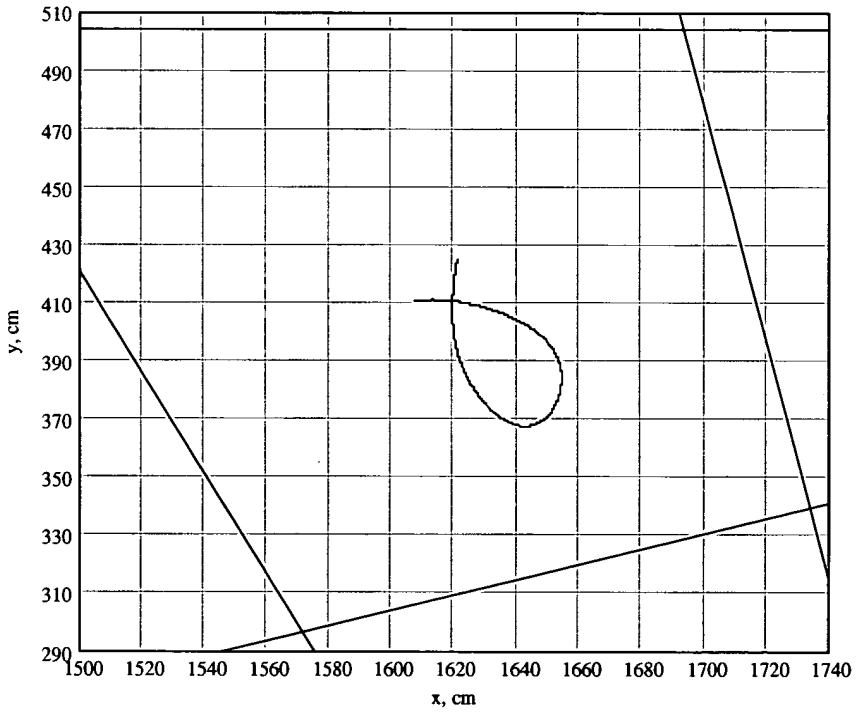

Fig. 28.8. The outline of the end cap in the right hollow

The curve obtained at these conditions is shown in Fig. 28.8. This curve crosses itself, too. It was used as a contour for a bulb-like cap in an additional peninsula-type adhesive joint (as shown in Fig. 28.2) located in the left part of the "Saturn" car's side airbag head protector.

Problem 3. Determine the shape of an isolated adhesive joint in the right part of the side curtain airbag head protector for the "Saturn" car.

The boundaries of the hollow in question are described in Table 18.

The intensity of the stress at the contour was assumed the same as before

(28.28) $U = \psi/p = 51.18$ mm.

The initial conditions were obtained by a careful exhaustive search in order to ensure the desirable contour's being a smooth closed curve.

(28.29) $x(0) = 1634.65$ mm;

(28.30) $y(0) = 397.83$ mm;

(28.31) $\phi(0) = 1.0377$.

Apparently, only one curve will be obtained for any particular intensity of the stress.

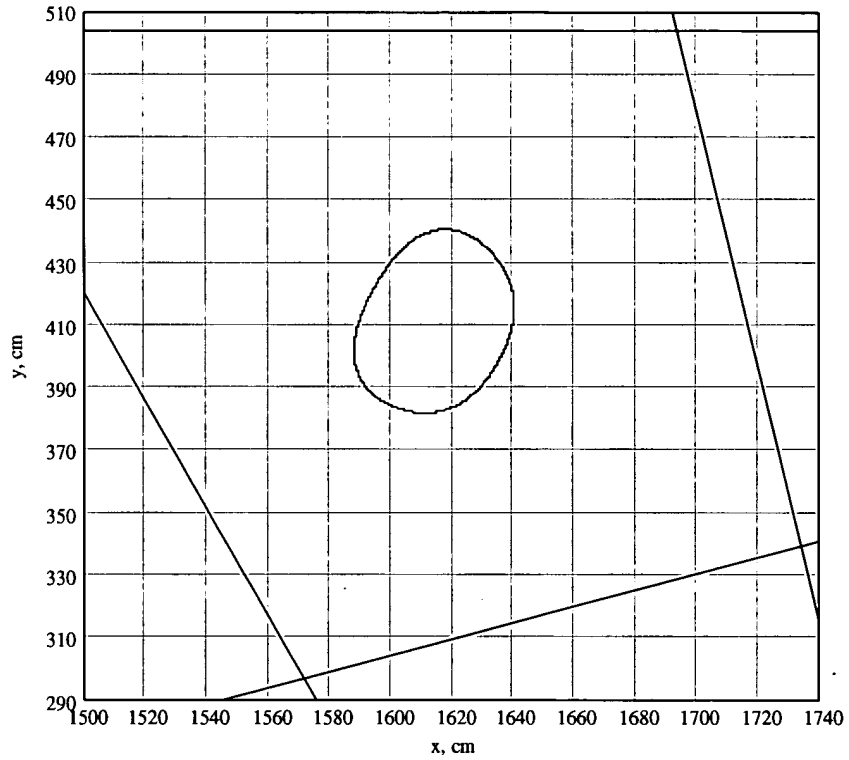

Fig. 28.9. The outlines of an isolated adhesive joint in the right hollow

The shape of the adhesive joint is shown in Fig. 28.9. This joint was not implemented when engineering the side curtain airbag for the "Saturn" car.

29. CORRECTION OF ADHESIVE JOINT'S SHAPE AFTER RESULTS OF FINITE ELEMENT ANALYSIS

A rational shape of an adhesive joint obtained by the inscribed circle technique makes the peeling stress along the joint's contour only approximately uniform. More accurate methods such as the finite element analysis are able to detect a non-uniformity in the stress distribution. The natural effect of this is that in some places of the contour the peeling stress can be greater than the rated design level specified for the joint. Immediately the idea comes to mind that the shape of the adhesive joint can be improved further so as to decrease the stress below the maximum allowed intensity.

This problem is addressed in the present chapter.

29.1. General idea of the method

In previous reports the shape of the adhesive joint is constructed using the basic formula

$$\psi = c_g c_l \frac{2pd}{\pi} f(\eta) \qquad (29.1)$$

where $\eta = \kappa d$;

ψ is the peeling stress;

p is the internal pressure above ambient;

d is the radius of an inscribed circle touching the joint's contour at the point of interest;

c_g is a global correction coefficient;

c_l is a local correction coefficient;

$f(\eta)$ is a function of a dimensionless parameter η defined as follows:

$$\begin{aligned} f(\eta) &= 1 + \frac{4}{5}\eta \qquad at \quad \eta \geq 0; \\ f(\eta) &= 1 + \frac{4}{5}\eta\left(1 - \frac{\eta^2}{3}\right) \qquad at \quad -1 \leq \eta < 0. \end{aligned} \qquad (29.2)$$

In earlier works, the correction coefficients c_g c_l were assumed equal to 1.

Here we propose to use a process of iterations to consecutively refine the shape of the joint. The description of the process follows. At the initial stage (iteration 0), the shape of the joint is determined as earlier with the given level of the peeling stress at the contour ψ_0 assuming $c_g = c_l = 1$. One has to solve the system of differential equations to do it:

$$x' = \cos\phi; \qquad (29.3)$$

$$y' = \sin\phi; \qquad (29.4)$$

$$\phi' = \frac{1}{d}\eta\left(\frac{\pi\psi_0}{2pd}\right); \qquad (29.5)$$

where x and y are Cartesian coordinates of the current point at the contour in question;

$\phi(s)$ is the angle between the positive direction of the x axis and that of the tangent to the contour;

η is an inverse function of f (29.2):

$$\begin{aligned} \eta(f) &= -2\cos\left[\frac{\pi + \alpha(f)}{3}\right] \qquad at \quad \frac{7}{15} \leq f < 1 \\ \eta(f) &= \frac{5}{4}(f - 1) \qquad at \quad 1 \leq f < \infty \end{aligned} \qquad (29.6);$$

where

$$\alpha(f) = \arccos\left[\frac{15}{8}(1 - f)\right]. \qquad (29.7)$$

Next, the airbag should be analyzed by the finite element technique to refine the intensity of the peeling stress along the joint's contour $\psi_1(s)$. This stress is a function of the arc coordinate s. If we assume this in the formula (3.36):

(29.8) $$c_g = 1;\ c_l(s) = c_1(s) = \frac{\psi_1(s)}{\psi_0};$$

then we can find the stress in the joint with the same result as that obtained by the finite element analysis.

Then, the first iteration of the contour's shape determination starts. To perform it, solve a system of differential equations:

(29.9) $$x' = \cos\phi;$$

(29.10) $$y' = \sin\phi;$$

(29.11) $$\phi' = \frac{1}{d}\eta\left(\frac{\pi\psi_1}{2c_1(s)\cdot pd}\right).$$

In this formula, ψ_1 is a new constant to be chosen in the course of solving the differential equation system. Its physical meaning is the new level of the peeling stress, uniform along the contour of the joint. Varying this constant will give a whole family of refined curves (Fig. 29.1). As dictated by logic, we should choose the one closest to the initial curve.

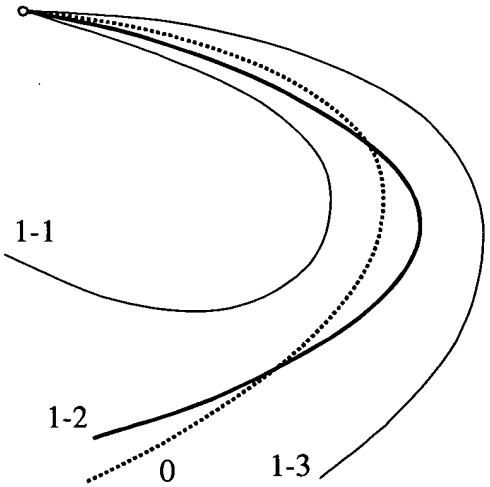

Fig. 29.1. Determination of the constant ψ_1. 0 is the initial shape of the contour; 1-1, 1-2, 1-3 are refined shapes obtained at different values of the ψ_1 constant.

The proximity of two curves (curve 0 and curve 1) specified parametrically by coordinates x_0, y_0; x_1, y_1 as functions of the arc length s can be characterized by the number K, the root-mean-square distance.

(29.12) $$K = \int_0^L \left((x_1(s) - x_0(s))^2 + (y_1(s) - y_0(s))^2\right) ds.$$

Here we assume, for the sake of definiteness, that the arc length coordinate can vary in the interval $[0, L]$.

Quite good results can be obtained also with a much simpler formula:

(29.13) $$D = (x_1(L) - x_0(L))^2 + (y_1(L) - y_0(L))^2.$$

The geometrical meaning of the number D is the squared distance between final points of the two curves.

Sometimes design considerations can be useful to choose the ψ_1 constant, such as the need to provide a desired width of the joint or a desired gap between adjacent joints.

The solution of the differential equation system (29.9) - (29.11) will give a new shape of the contour. With this one, again we do the finite element analysis to find the new stress $\psi_2(s)$. As assumed, this new stress should be closer to the specified level ψ_1. Taking the local coefficient as

$$c_2(s) = c_1(s)\frac{\psi_2(s)}{\psi_1}; \qquad (29.14)$$

we use the formula

$$\psi = c_2(s)\frac{2pd}{\pi} f(\eta) \qquad (29.15)$$

to find the peeling stress in the current joint, and the result is going to be the same as that calculated by the finite element analysis.

The process of iterations can be continued, and at the i-th iteration this system of equations must be solved:

$$x' = \cos\phi; \qquad (29.16)$$

$$y' = \sin\phi; \qquad (29.17)$$

$$\phi' = \frac{1}{d}\eta\left(\frac{\pi\psi_i}{2c_i(s)\cdot pd}\right); \qquad (29.18)$$

where

$$c_i(s) = c_{i-1}(s)\frac{\psi_i(s)}{\psi_{i-1}}; \qquad (29.19)$$

$$c_0(s) = 1. \qquad (29.20)$$

$\psi_i(s)$ is the distribution of the peeling stress along the contour determined by the finite element analysis for the contour constructed at $(i - 1)$-th iteration.

The process of iterations can be finished when the stress $\psi_i(s)$ is close enough to the given level ψ_i:

$$\frac{|\psi_i(s) - \psi_i|}{\psi_i} \le \varepsilon; \qquad (29.21)$$

where ε is a given relative accuracy of the analysis, for example, $\varepsilon = 0.2$.

The convergence of the process should be checked by experimentation.

The relationships for $\psi_i(s)$ obtained by the finite element analysis can be non-smooth or saw-toothed. Therefore, before substituting these relationships to the formulae (29.8), (29.12), (29.19), they should be smoothed somehow.

29.2. A test problem

The test problem for this section will be one from chapter 26. It conforms to the geometry shown in Fig. 29.3. The dimensions are following: a = 5.5 cm, b = 7.5 cm, c = 2.5 cm.

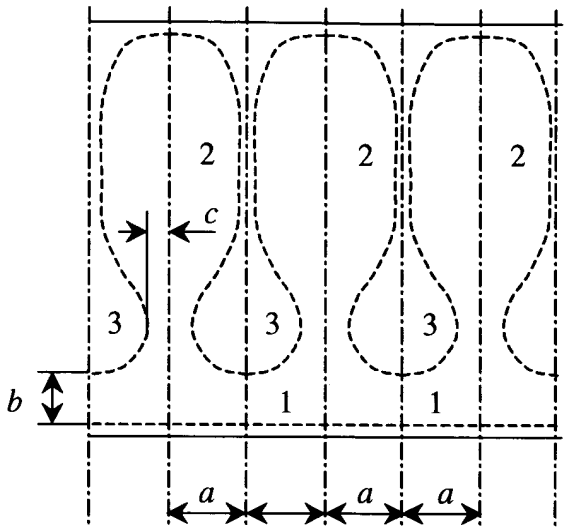

Fig. 29.2. An adhesive joint between two film sheets at intersections of long hollows
(1) a straight-edge hollow; (2) a bilaterally symmetrical hollow;
(3) an adhesive joint area

A rational shape has been determined at the internal pressure above ambient p = 0.5 kg/cm^2, the peeling stress at this contour is 2.559 kg/cm.

The same problem has been solved using the finite element method. The peeling stress has been calculated in 24 points shown in Fig. 29.3.

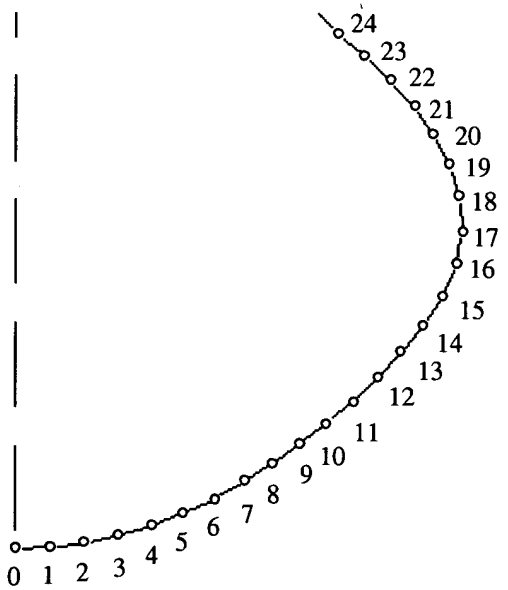

Fig. 29.3. Points at the contour of the adhesive joints

Results of the finite element analysis are shown as a red line plot in Fig. 29.4. This plot is the basis for determining the local coefficient $c_1(s)$ at the first iteration. The line has teeth, therefore the further analysis uses a smoothed relationship (the blue line on the figure) obtained by the function *ksmooth* in the Mathcad-2000 software with the smoothing interval equal to three distances between adjacent points.

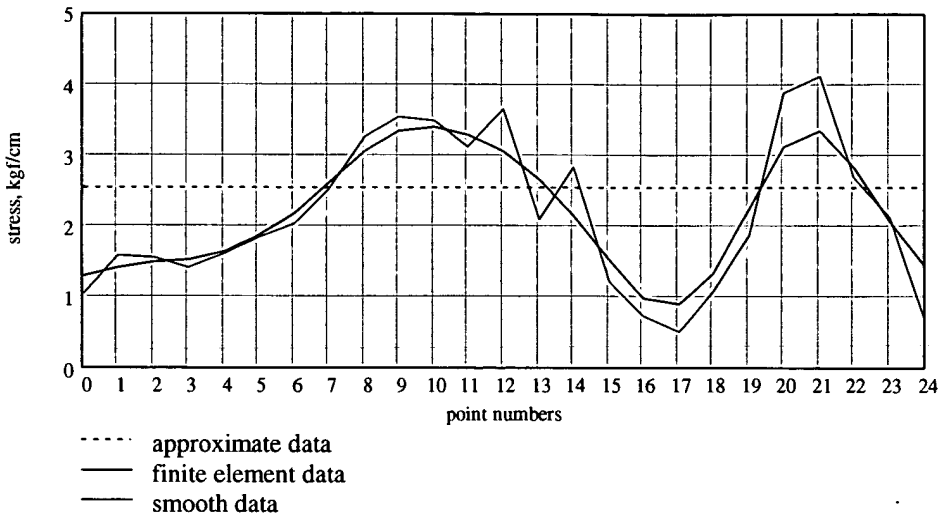

Fig. 29.4. Plots of the peeling stress at the contour, at the first iteration $\psi_1(s)$

The plot of the local coefficient $c_1(s)$ calculated by the formula (29.8) is presented in Fig. 29.5.

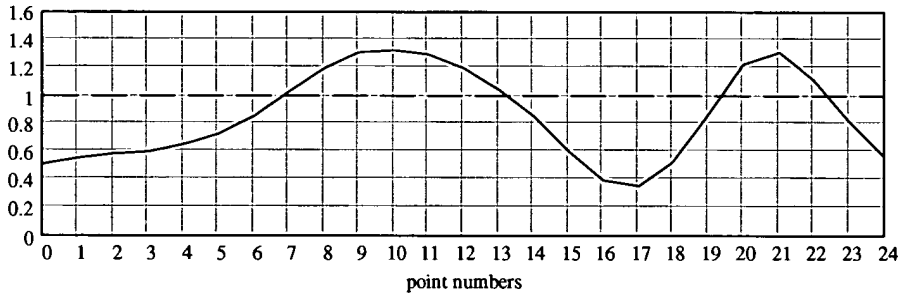

Fig. 29.5. Local coefficient $c_1(s)$

On the basis of this relationship and the solution of the differential equation system (29.9) - (29.11), a new shape of the contour has been obtained (Fig. 29.6). The intensity of the peeling stress ψ_1 is assumed to be 1.984 which provides the half-width of the channel equal to $c = 2.5$ cm.

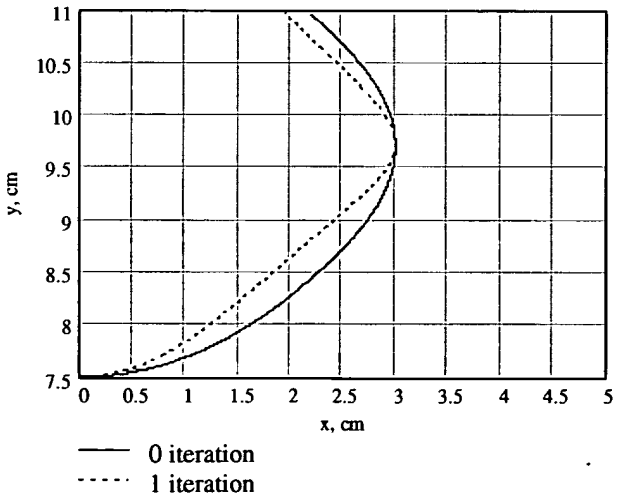

Fig. 29.6. The contour of the adhesive joint at zero and first iterations

The new shape of the contour is different from the old one in that it has a small rounding radius in areas with folds (points 0 and 17 in Fig. 29.3) while it is almost straight in regions far from those areas.

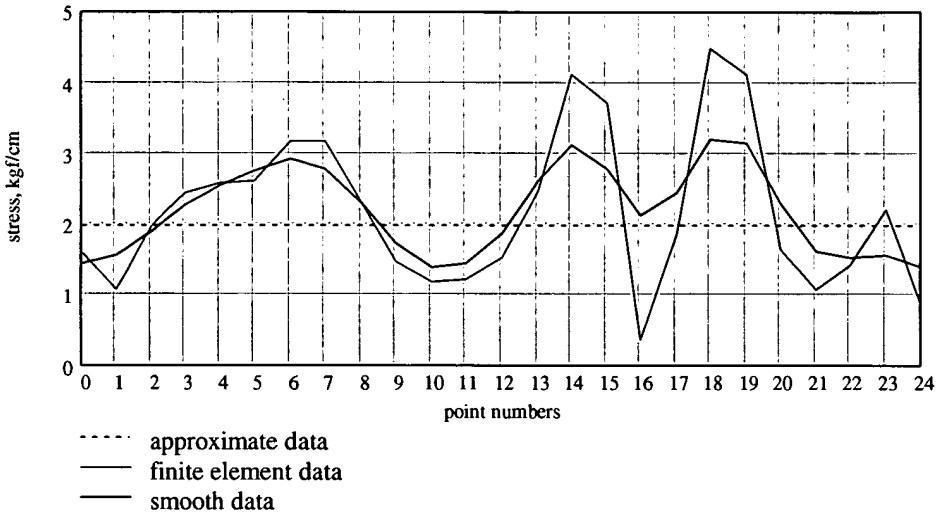

Fig. 29.7. Plots of the peeling stress at the contour after 1st iteration, $\psi_2(s)$

Next, the finite element analysis has been performed for the airbag with the new outline of the adhesive joint. The result of this analysis is presented in Fig. 29.8.

The same figure presents a smoothed curve (blue line) used for determining the local coefficient $c_2(s)$ by the formula (29.14) or (29.19).

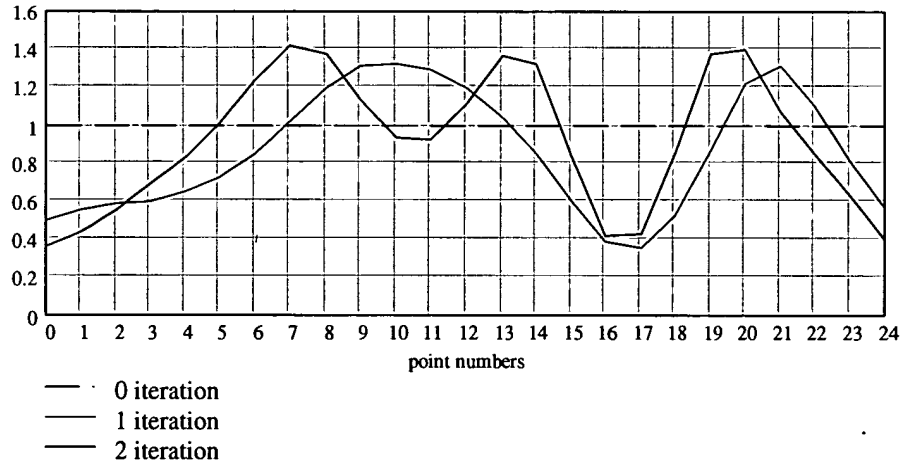

Fig. 29.8. Plots of local coefficients $c_0(s)$, $c_1(s)$, $c_2(s)$

For the sake of comparison, this figure also presents plots of the local coefficients $c_0(s)$ and $c_1(s)$.

On the basis of the $c_2(s)$ relationship and the solution of the differential equation system (29.16) - (29.18), a new shape of the joint has been then obtained (Fig. 29.9). The peeling stress ψ_2 is 2.072 to provide the half-width of the channel equal to $c = 2.5$ cm.

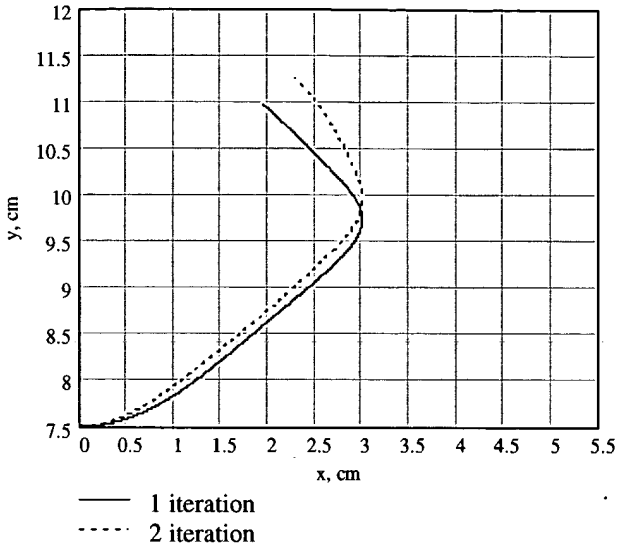

Fig. 29.9. The contour of the joint at 1st and 2nd iterations

The shape of the contour has changed a bit. Though, it has kept its characteristic property of having small rounding radii in fold formation areas.

The analysis of the safety airbag with this new shape of the joint gave the results shown in Fig. 29.10.

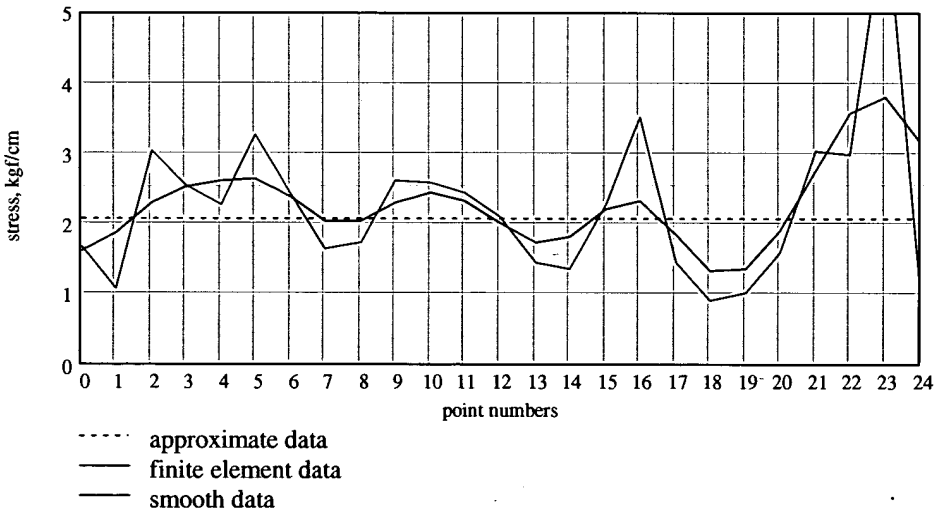

Fig. 29.10. Plots of the peeling stress at the contour after the second iteration, $\psi_3(s)$

The character of these data shows that "noise" due to inaccuracies in the finite element approximation and other factors is comparable to the deviation of the curve from its perfect horizontal position. Further iterations make sense only with a finer finite-element mesh.

Nonetheless, we have calculated the coefficient $c_3(s)$ for the next iteration. Its plot is shown in Fig. 29.11.

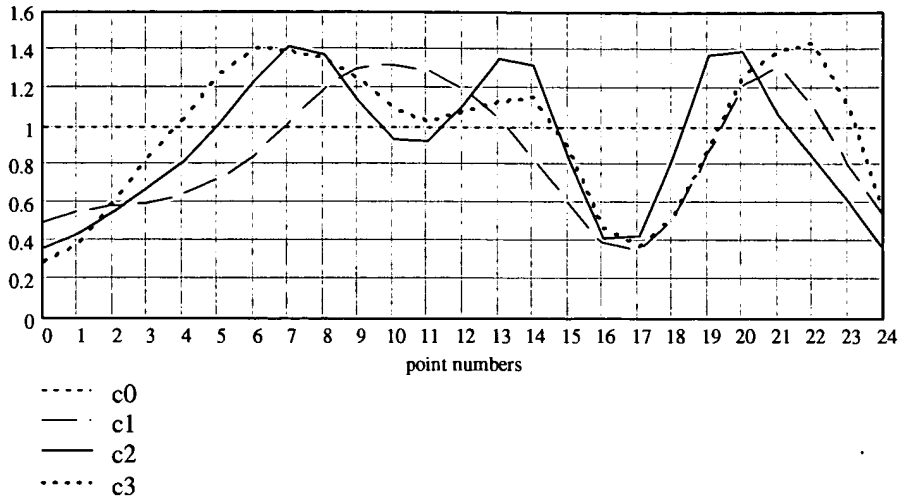

Fig. 29.11. Local coefficients $c_0(s)$, $c_1(s)$, $c_2(s)$, $c_3(s)$

For the purpose of comparison, the same figure presents plots of coefficients obtained at the previous iterations.

30. REFERENCES

[24]. Appendix 4. Deformed shape and stress state of side head protectors.

[25]. Appendix 5. Approximate method to determine the peeling stress.